# All-optical electrophysiology in mammalian neurons using engineered microbial rhodopsins

Daniel R Hochbaum[1,16], Yongxin Zhao[2,16], Samouil L Farhi[3], Nathan Klapoetke[4–7], Christopher A Werley[3], Vikrant Kapoor[8], Peng Zou[3], Joel M Kralj[3], Dougal Maclaurin[9], Niklas Smedemark-Margulies[3], Jessica L Saulnier[10], Gabriella L Boulting[10], Christoph Straub[10], Yong Ku Cho[4–7], Michael Melkonian[11], Gane Ka-Shu Wong[12–14], D Jed Harrison[2], Venkatesh N Murthy[8], Bernardo L Sabatini[10,15], Edward S Boyden[4–7,17], Robert E Campbell[2,17] & Adam E Cohen[3,9,15]

All-optical electrophysiology—spatially resolved simultaneous optical perturbation and measurement of membrane voltage—would open new vistas in neuroscience research. We evolved two archaerhodopsin-based voltage indicators, QuasAr1 and QuasAr2, which show improved brightness and voltage sensitivity, have microsecond response times and produce no photocurrent. We engineered a channelrhodopsin actuator, CheRiff, which shows high light sensitivity and rapid kinetics and is spectrally orthogonal to the QuasArs. A coexpression vector, Optopatch, enabled cross-talk–free genetically targeted all-optical electrophysiology. In cultured rat neurons, we combined Optopatch with patterned optical excitation to probe back-propagating action potentials (APs) in dendritic spines, synaptic transmission, subcellular microsecond-timescale details of AP propagation, and simultaneous firing of many neurons in a network. Optopatch measurements revealed homeostatic tuning of intrinsic excitability in human stem cell–derived neurons. In rat brain slices, Optopatch induced and reported APs and subthreshold events with high signal-to-noise ratios. The Optopatch platform enables high-throughput, spatially resolved electrophysiology without the use of conventional electrodes.

To disentangle the complex interactions underlying neural dynamics, it is desirable to visualize membrane voltage across spatial scales, from single dendritic spines to large numbers of interacting neurons, while delivering spatially and temporally precise stimuli[1,2]. Optical methods for simultaneous perturbation and measurement of membrane potential could achieve this goal[3].

Genetic targeting is particularly important for the stimulation and recording of specific cells in intact tissue where closely spaced cells often perform distinct functions. Genetic targeting is also valuable *in vitro*, for characterizing heterogeneous cultures that arise during stem cell differentiation to neurons[4] or while studying neurons cultured with other cell types.

Optical stimulation has been demonstrated with glutamate uncaging[5], photoactivated ion channel agonists[6] and microbial rhodopsin actuators[7]. Genetically encoded functional readouts include reporters of intracellular $Ca^{2+}$ and membrane voltage[8]. Voltage-sensitive dyes offer good speed, sensitivity and spectral tuning[9,10] but cannot be delivered to a genetically specified subset of cells and often suffer from phototoxicity.

Optical stimulation has been paired with voltage imaging[11–14]. However, robust and cross-talk–free genetically targeted all-optical electrophysiology has not been achieved owing to limitations on the speed and sensitivity of genetically encoded voltage indicators (GEVIs) and because of spectral overlap between existing GEVIs and optogenetic actuators. GFP-based GEVIs experience severe optical cross-talk with even the most red-shifted channelrhodopsins, which retain ~20% activation with blue light excitation[15]. Sensitive, fast and spectrally orthogonal tools are needed for genetically targeted simultaneous optical perturbation and measurement of membrane voltage.

Here we introduce variants of a near-infrared archaerhodopsin-based voltage indicator and a blue light–gated channelrhodopsin actuator that individually show greatly improved

[1]Applied Physics Program, School of Engineering and Applied Science, Harvard University, Cambridge, Massachusetts, USA. [2]Department of Chemistry, University of Alberta, Edmonton, Alberta, Canada. [3]Department of Chemistry and Chemical Biology, Harvard University, Cambridge, Massachusetts, USA. [4]The MIT Media Laboratory, Massachusetts Institute of Technology (MIT), Cambridge, Massachusetts, USA. [5]Department of Biological Engineering, MIT, Cambridge, Massachusetts, USA. [6]Department of Brain and Cognitive Sciences, MIT, Cambridge, Massachusetts, USA. [7]McGovern Institute for Brain Research, MIT, Cambridge, Massachusetts, USA. [8]Department of Molecular and Cellular Biology, Harvard University, Cambridge, Massachusetts, USA. [9]Department of Physics, Harvard University, Cambridge, Massachusetts, USA. [10]Department of Neurobiology, Harvard Medical School, Boston, Massachusetts, USA. [11]Institute of Botany, Cologne Biocenter, University of Cologne, Cologne, Germany. [12]Department of Biological Sciences, University of Alberta, Edmonton, Alberta, Canada. [13]Department of Medicine, University of Alberta, Edmonton, Alberta, Canada. [14]Beijing Genomics Institute–Shenzhen, Shenzhen, China. [15]Howard Hughes Medical Institute, Harvard University, Cambridge, Massachusetts, USA. [16]These authors contributed equally to this work. [17]These authors jointly directed this work. Correspondence should be addressed to A.E.C. (cohen@chemistry.harvard.edu).
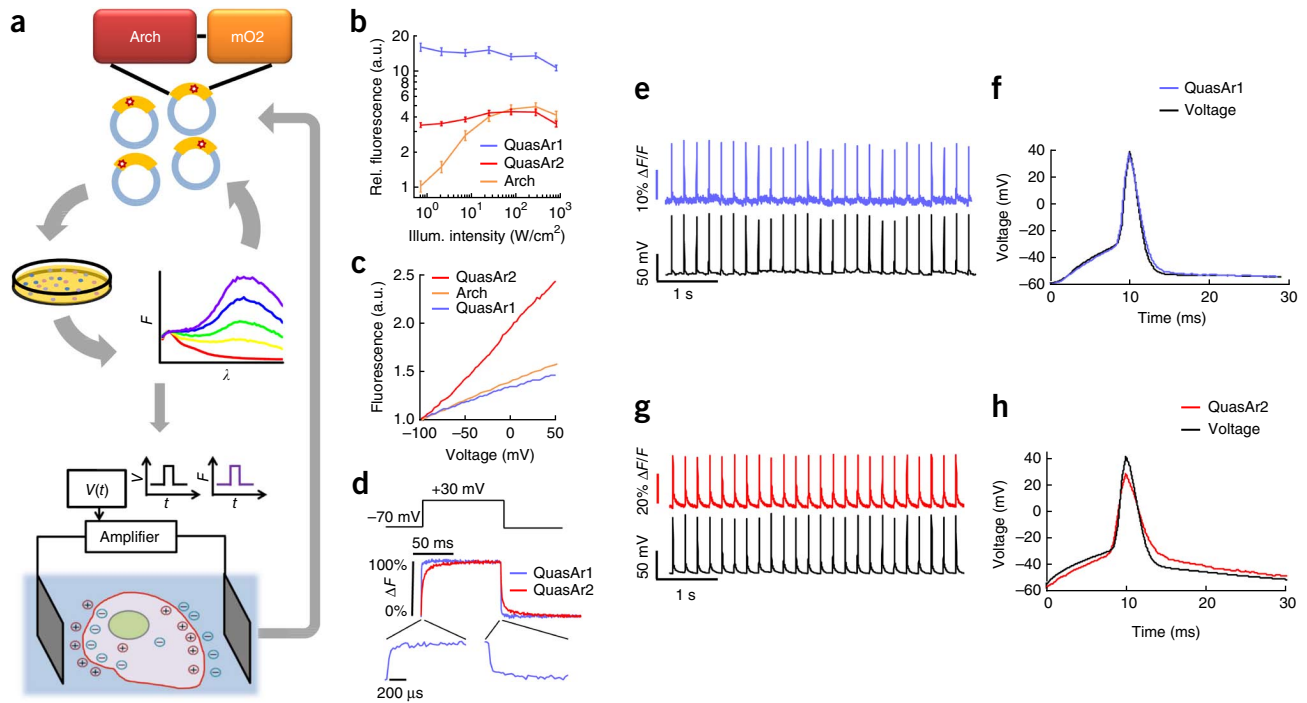
**Figure 1** | Nonpumping Arch-derived voltage indicators with improved speed, sensitivity and brightness. (**a**) Hierarchical screen to select improved Arch mutants. Five rounds of random mutagenesis and screening for brightness were performed in *E. coli*. The brightest mutants were subjected to targeted mutagenesis and screening for speed and voltage sensitivity in HeLa cells via induced transient voltage (**Supplementary Fig. 1**). (**b**) Fluorescence of Arch and QuasAr mutants fused to EGFP and expressed in HEK cells, as a function of illumination intensity. The fluorescence of Arch and each mutant is normalized by 640-nm illumination intensity and by EGFP fluorescence. A linear fluorophore would appear as a horizontal line. Error bars, s.e.m. (*n* = 7 cells for each mutant). a.u., arbitrary units. (**c**) Fluorescence vs. membrane voltage for Arch, QuasAr1 and QuasAr2 expressed in HEK cells. (**d**) Fluorescence responses to a step in membrane voltage from −70 to +30 mV. (**e**) Simultaneous optical and electrical recording of APs in a rat hippocampal neuron expressing QuasAr1. Frame rate, 1 kHz. (**f**) Overlay of mean optically and electrically recorded AP waveforms. Frame rate, 2 kHz. (**g,h**) Same as **e,f**, in neurons expressing QuasAr2. Data in **b**–**h** acquired on a 128 × 128–pixel electron-multiplying charge-coupled device (EMCCD) camera.

performance relative to published optogenetic tools and that together constitute a tool for all-optical electrophysiology. First, we characterized the optical and electrophysiological properties of the indicator, actuator and coexpressed pair (Optopatch) and compared against those of published tools. Second, we used Optopatch to probe neuronal excitation across spatial and temporal scales: from single dendritic spines to fields containing dozens of neurons measured in parallel, and from microsecond delays associated with AP propagation to days-long changes in excitability. Third, we applied Optopatch to study excitability in human induced pluripotent stem cell (hiPSC)-derived neurons. These measurements revealed the first evidence for homeostatic plasticity of intrinsic excitability in hiPSC-derived neurons. Fourth, we applied Optopatch in tissue. In organotypic brain slice, Optopatch initiated and reported APs and subthreshold dynamics with higher signal-to-noise ratios (SNRs), better photostability and better time resolution than ArcLight, a recently introduced GFP-based GEVI[16].

## RESULTS

### Directed evolution of an Arch-based voltage indicator

We previously showed that archaerhodopsin 3 (Arch) functions as a fast and sensitive voltage indicator[17]. Arch has the furthest red-shifted spectrum of any GEVI, giving it the unique property of little spectral overlap with channelrhodopsin actuators and GFP-based reporters. Thus it is natural to pair Arch-based

indicators with optogenetic actuators for cross-talk–free all-optical electrophysiology.

However, wild-type Arch had some undesirable attributes for a reporter: it was very dim, and the brightness was a nonlinear function of illumination intensity[18]. Illumination for imaging generated a hyperpolarizing photocurrent, which partially suppressed neural firing. The mutant Arch(D95N) did not pump, but its step response was dominated by a 41-ms time constant—too slow to resolve AP waveforms. Other nonpumping mutants improved speed relative to Arch(D95N) but did not reach the speed of wild-type Arch and did not address the low brightness[14].

We sought to repair these defects in engineered mutants of Arch. To accommodate the multiple selection criteria, we adopted a hierarchical screen (**Fig. 1a**). Five rounds of brightness screening in *Escherichia coli* and random mutagenesis on a library of >10⁴ Arch mutants resulted in a brighter Arch variant, containing five point mutations (Online Methods). Further site-directed mutagenesis at known key residues improved voltage sensitivity and speed (**Supplementary Fig. 1**), and addition of an endoplasmic reticulum export motif and a trafficking sequence improved targeting to the plasma membrane. The two most promising mutants were named QuasArs ('quality superior to Arch'). QuasAr1 differed from wild-type Arch by the mutations P60S, T80S, D95H, D106H and F161V. QuasAr2 differed from QuasAr1 by the mutation H95Q. Both proteins had fluorescence excitation maxima at 590 nm and emission maxima at 715 nm

(**Supplementary Fig. 2**). The fluorescence quantum yields of solubilized QuasAr1 and QuasAr2 were 19- and 10-fold enhanced, respectively, relative to that of the nonpumping voltage indicator Arch(D95N) (**Supplementary Table 1**). For fluorescence microscopy of QuasArs, we used 640-nm excitation.

We compared the fluorescence, voltage sensitivity and speed of the QuasArs to those of wild-type Arch in human embryonic kidney (HEK) cells, using epifluorescence microscopy and whole-cell patch-clamp electrophysiology. Under low-intensity illumination (500 mW/cm$^2$), QuasAr1 was 15-fold brighter than wild-type Arch, and QuasAr2 was 3.3-fold brighter (**Fig. 1b**). Neither mutant showed the optical nonlinearity seen in the wild-type protein, implying that fluorescence was a one-photon process with the voltage-sensitive transition occurring from the ground state. At high intensity (>100 W/cm$^2$), QuasAr1 was 2.5-fold brighter than wild-type Arch, whereas QuasAr2 and of wild-type Arch had comparable brightness.

Fluorescence, $F$, of Arch, QuasAr1 and QuasAr2 increased nearly linearly with membrane voltage between −100 mV and +50 mV (**Fig. 1c**). Sensitivities were (as $\Delta F/F$ per 100 mV): 32% ± 3% for QuasAr1 ($n = 5$ cells; all statistics are mean ± s.e.m. unless specified) and 90% ± 2% for QuasAr2 ($n = 6$ cells). The sensitivity of QuasAr2 was substantially improved over those of both Arch (40% per 100 mV) and Arch(D95N) (60% per 100 mV).

Steps in membrane voltage (−70 mV to +30 mV) induced rapid fluorescence responses in both mutants, which we quantified on a fast photomultiplier (**Fig. 1d**). At room temperature (23 °C), QuasAr1 had a step-response time constant of 0.053 ± 0.002 ms ($n = 6$ cells), close to the 0.05-ms time resolution of the electronics and substantially faster than the 0.6-ms step response of wild-type Arch[18]. QuasAr2 had a biexponential step response with time constants of 1.2 ± 0.1 ms (68%) and 11.8 ± 1.5 ms (32%) ($n = 6$ cells). At 34 °C, the apparent speed of QuasAr1 remained at the 0.05-ms resolution of the electronics, and the time constants of QuasAr2 decreased to 0.30 ± 0.05 ms (62%) and 3.2 ± 0.4 ms (38%) ($n = 7$ cells). Both mutants had similar response times on rising and falling edges (**Supplementary Table 2**). Neither QuasAr1 nor QuasAr2 generated detectable photocurrent under red light (tested up to 900 W/cm$^2$) or blue light (**Supplementary Fig. 3**).

We expressed QuasArs in cultured rat hippocampal neurons, evoked APs and recorded the fluorescence responses from the soma and proximal dendrites (1-kHz frame rate; **Fig. 1e–h** and **Supplementary Fig. 4**). Single APs produced fluorescence transients with amplitude $\Delta F/F = 21\% \pm 2\%$ for QuasAr1 ($n = 11$ cells) and $\Delta F/F = 48\% \pm 3\%$ for QuasAr2 ($n = 24$ cells). SNRs for single APs increased with illumination intensity. For QuasAr1, SNR values were 21 ± 2 (300 W/cm$^2$, $n = 6$ cells) and 32 ± 4 (800 W/cm$^2$, $n = 6$ cells). For QuasAr2, SNR values were 41 ± 4 (300 W/cm$^2$, $n = 12$ cells) and 70 ± 8 (800 W/cm$^2$, $n = 12$ cells). These SNRs correspond to equivalent electrical noise levels of approximately 3.0 and 4.3 mV (at 800 and 300 W/cm$^2$, respectively) for QuasAr1 and of 1.5 and 2.2 mV (for 800 and 300 W/cm$^2$, respectively) for QuasAr2.

QuasAr1 did not introduce detectable broadening in the optically recorded AP waveform, acquired at a 2-kHz frame rate (**Fig. 1f**). At room temperature, QuasAr2 broadened the optically recorded AP by 650 ± 150 µs relative to the simultaneously recorded electrical waveform at 70% maximum depolarization ($n = 5$ cells; mean ± s.d.) (**Fig. 1h**). At 34 °C, QuasAr2 broadened

the optically recorded AP by 180 ± 120 µs ($n = 5$ cells; mean ± s.d.). Both probes reported AP peak times with <100-µs jitter relative to simultaneously acquired patch clamp recordings.

Photostability is a concern with any voltage indicator, so we quantified the stability of QuasArs under continuous illumination at standard imaging intensity (300 W/cm$^2$). Photobleaching time constants were 440 s for QuasAr1 and 1,020 s for QuasAr2. We further tested for red light–induced phototoxicity using QuasAr2 as the readout. Under continuous illumination at 300 W/cm$^2$, QuasAr2 reported APs with 100% fidelity for the 30-min duration of the experiment, with no detectable change in AP width or waveform (**Supplementary Fig. 5**).

We compared the QuasArs to ArcLight A242 (ref. 16). Photophysical comparisons were performed in HEK cells (**Supplementary Table 2**), and AP comparisons were performed in matched neuronal cultures. ArcLight can be imaged with ~30-fold lower illumination intensity than is required for the QuasArs, facilitating measurements on readily available microscope systems. However, the QuasArs reported APs with 7- to 16-fold larger fractional fluorescence changes, 3- to 8-fold higher SNR, 30- to 1,000-fold higher temporal resolution and 6- to 15-fold greater photostability (**Supplementary Fig. 6**).

The QuasArs represent, to our knowledge, the fastest and most sensitive GEVIs reported to date. The 50-µs response time of QuasAr1 is more than tenfold faster than the fastest previously reported GEVIs[18,19] and is comparable to fast voltage-sensitive dyes. QuasAr1 opens the possibility of accurate mapping of AP waveforms for even the fastest-spiking neurons[20]. The QuasArs report voltage with greatly improved sensitivity and time resolution compared to the first generation of Arch-based GEVIs, despite requiring about fivefold lower illumination intensity[17]. From a signal-to-noise perspective, QuasAr2 is superior to QuasAr1: the greater voltage sensitivity of QuasAr2 outweighs the greater brightness of QuasAr1. From a temporal resolution perspective, QuasAr1 is superior. We recommend QuasAr2 for spike counting and measurement of subthreshold events, and QuasAr1 for measurement of microsecond-precision AP waveforms and timing. Furthermore, the far-red excitation of the QuasArs allows, in principle, combination with channelrhodopsin actuators or other GFP-based reporters.

## CheRiff, a sensitive blue-shifted optogenetic actuator

We next sought to combine the QuasAr reporters with a blue light–activated channelrhodopsin. To achieve spatially precise optical excitation, the channelrhodopsin should trigger APs when only a subsection of a cell is excited. Existing optogenetic actuators have had only marginal success in achieving this goal[21]. To avoid optical cross-talk, the blue light intended for the channelrhodopsin should not interfere with the GEVI fluorescence. Existing optogenetic actuators require blue light intensities that spuriously increase QuasAr fluorescence (**Supplementary Fig. 7**). We thus sought a more sensitive channelrhodopsin that could reliably trigger APs with subcellular illumination and at lower light intensity while maintaining fast opening and closing kinetics.

During a screen of plant genomes[22], we identified a novel optogenetic actuator, *Scherffelia dubia* channelrhodopsin (sdChR)[15], derived from a freshwater green alga first isolated from a small pond in Essex, England[23] (**Supplementary Fig. 8**).

**Figure 2** | CheRiff is a fast and sensitive blue-shifted channelrhodopsin. (**a**) Action spectrum acquired in HEK293T cells ($n$ = 6 cells). CheRiff had a blue-shifted action spectrum with a peak at $\lambda_{exc}$ of ~460 nm. a.u., arbitrary units. (**b**) Cultured rat hippocampal neuron expressing CheRiff-EGFP, imaged via EGFP fluorescence. Scale bar, 25 μm. Image acquired on a scientific complementary metal-oxide semiconductor (sCMOS) detector. (**c**) Comparison of photocurrents as a function of illumination intensity in matched neuronal cultures expressing CheRiff ($n$ = 5 cells) or ChR2 H134R ($n$ = 5 cells). Illumination was either over the whole cell or confined to the soma. Dotted lines indicate whole-cell illumination intensities at which photocurrents reach 1 nA. (**d**) Spiking fidelity as a function of stimulation frequency and illumination intensity in neurons expressing CheRiff ($n$ = 5 cells). Cells were stimulated with trains of 40 pulses (2-ms pulse width, 10–80 Hz) at three different blue light intensities. Error bars (**a**,**c**,**d**), s.e.m.



sdChR had promising sensitivity and a blue action spectrum (peak excitation wavelength $\lambda_{max}$ = 474 nm). Addition of a trafficking sequence improved membrane targeting (**Supplementary Fig. 8**). Introduction of the mutation E154A sped the kinetics and shifted the peak of the action spectrum to $\lambda_{max}$ = 460 nm (**Fig. 2a**), which decreased spurious channelrhodopsin activation by red light (**Supplementary Fig. 9** and **Supplementary Table 3**). We dubbed the final construct CheRiff in reference to *Scherffelia*, its genus of origin. CheRiff showed good expression and membrane trafficking in cultured rat hippocampal neurons (**Fig. 2b**).

Under typical neural culture conditions, rapid and robust AP initiation requires currents of approximately 1 nA (ref. 24). In a paired comparison, CheRiff passed a photocurrent of 1 nA at a whole-cell illumination intensity of $22 \pm 10$ mW/cm$^2$ ($n$ = 5 neurons), ninefold lower than was required for channelrhodopsin 2 (ChR2) H134R ($200 \pm 80$ mW/cm$^2$, $n$ = 5 neurons) (**Fig. 2c**). For stimulation localized to the soma, CheRiff passed a photocurrent of 1 nA under illumination at 100 mW/cm$^2$, whereas ChR2 H134R did not achieve this photocurrent under any illumination intensity. Upon pulsed whole-cell illumination, CheRiff induced high-frequency and high-reliability spike trains (**Fig. 2d**) at five- to tenfold lower illumination intensities than have been reported for ChR2 H134R, ChIEF or ChETA[24] using the same protocol.

We measured the photophysical properties of CheRiff, ChR2 H134R and ChIEF[25] in matched neuronal cultures (**Supplementary Fig. 9** and **Supplementary Table 4**). CheRiff showed twofold larger maximal photocurrents than ChR2 H134R or ChIEF. CheRiff had an opening rate twofold faster than that of ChR2 H134R and fourfold faster than that of ChIEF. CheRiff had a similar closing rate to that of ChIEF and was 1.5-fold faster than ChR2 H134R.

Finally, we tested for optical cross-talk between QuasArs and CheRiff in cultured neurons (**Supplementary Table 5**). Illumination sufficient to induce high-frequency trains of APs (488 nm, 140 mW/cm$^2$) perturbed fluorescence of QuasArs by <1% (**Supplementary Fig. 7**). Illumination with high-intensity red light (640 nm, 900 W/cm$^2$) induced an inward photocurrent through CheRiff of $14.3 \pm 3.1$ pA, which depolarized neurons by $3.1 \pm 0.2$ mV ($n$ = 5 cells) (**Supplementary Fig. 9**). For most applications, this level of optical cross-talk is acceptable.

Of the many attributes that determine channelrhodopsin function, the most important in CheRiff are its greatly increased sensitivity at low illumination intensity and its fast opening kinetics. These properties allow sub-cellular and low-intensity triggering of precisely timed APs.
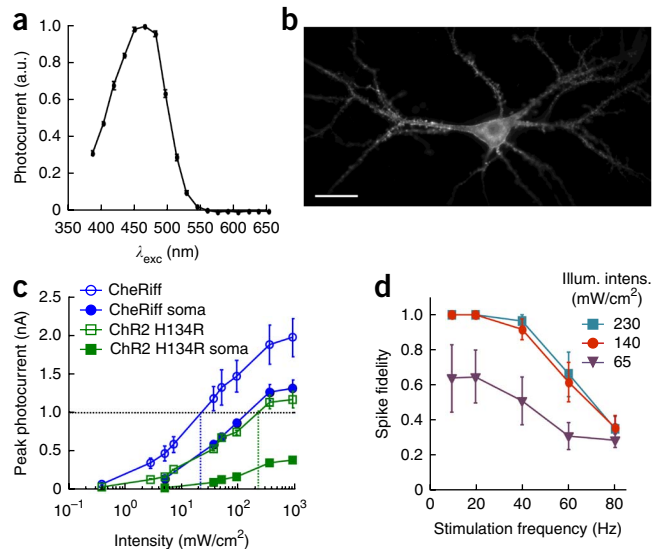
## Optopatch constructs

Optopatch1 and Optopatch2 consisted of bicistronic vectors for coexpression of CheRiff-EGFP and QuasAr1- or QuasAr2-mOrange2, respectively (**Supplementary Fig. 10**). We also made Optopatch variants that contained nonfluorescent EGFP and mOrange2 mutants, thereby freeing the spectrum for other uses. The QuasAr and CheRiff constructs could also be delivered separately, but the bicistronic vector maintained a more uniform ratio of actuator-to-reporter expression levels.

We characterized Optopatch2 in detail. When expressed under a *CaMKIIα* (*Camk2a*) promoter in cultured rat hippocampal neurons, Optopatch2 showed high expression and good membrane trafficking of both CheRiff and QuasAr2 (**Fig. 3a**). Patch-clamp measurements found no statistically significant effect of expression on membrane resistance ($P$ = 0.72, two-tailed student's $t$-test), membrane capacitance ($P$ = 0.87), resting potential ($P$ = 0.31), threshold current ($P$ = 0.67) or threshold potential ($P$ = 0.38) when compared to paired cultures transfected with cytoplasmic GFP driven by a *CaMKIIα* promoter ($n$ = 8 cells for Optopatch2, $n$ = 7 cells for GFP) (**Supplementary Fig. 11**).

A neuron expressing Optopatch2 was exposed to whole-field illumination with pulses of blue light (10 ms, 25 mW/cm$^2$) to stimulate CheRiff and to simultaneous constant illumination with red light (800 W/cm$^2$) to excite fluorescence of QuasAr2. We imaged fluorescence of QuasAr2 at a 1-kHz frame rate and calculated fluorescence from whole-cell average intensity (**Supplementary Fig. 4**) while simultaneously recording membrane voltage via a patch pipette. The optical and electrical traces corresponded closely (**Fig. 3b**).

Raw movies acquired at 1 kHz clearly showed fluorescence changes due to optically triggered APs (**Supplementary Video 1**). Averaging temporally registered AP movies over multiple trials improved the SNR for subcellular AP mapping (**Supplementary Video 2**). Under focused red illumination (2,200 W/cm$^2$), back-propagating APs were detected in single dendritic spines on a single-trial basis with an SNR of 2.5 (**Fig. 3c**).

## Probing synaptic transmission

With Optopatch, one can stimulate and record from independently selected and rapidly reconfigured regions of a neural circuit. We implemented this capability in culture using a digital micromirror
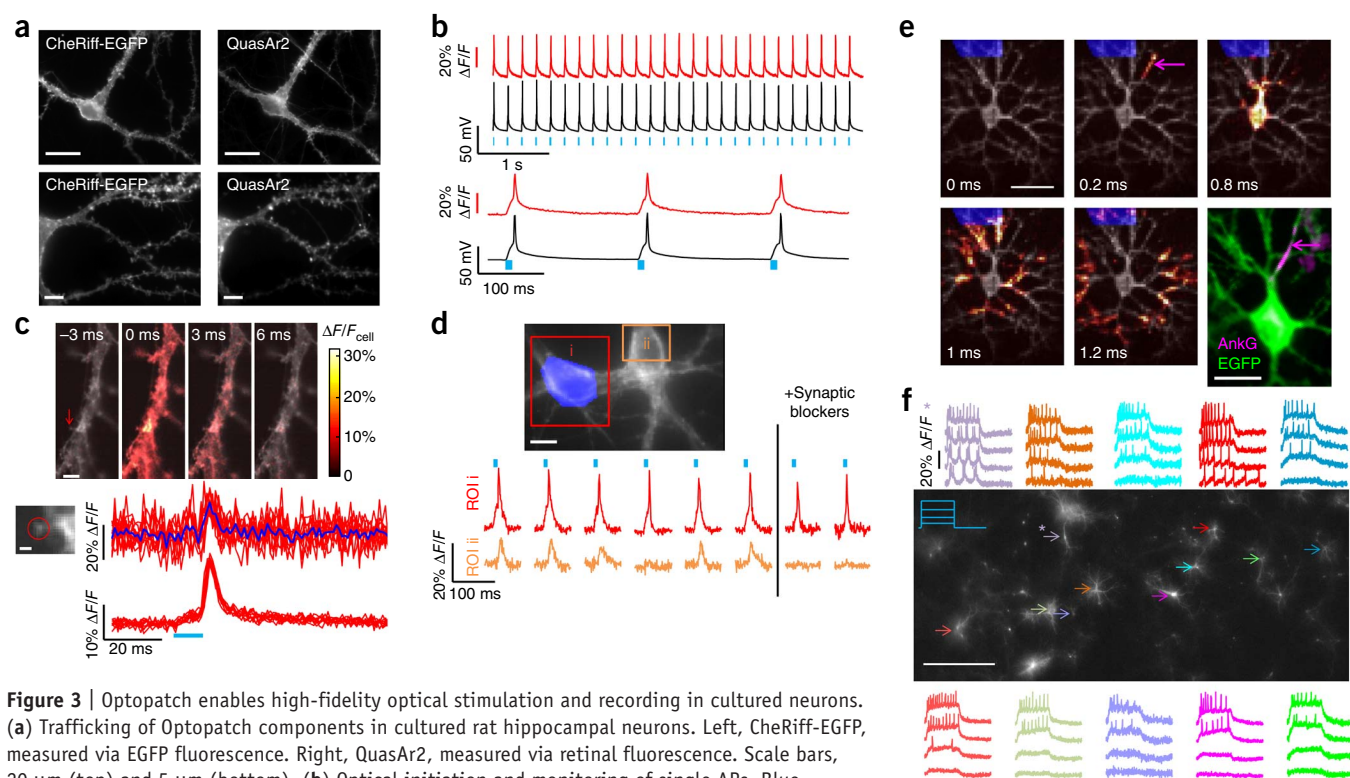
**Figure 3** | Optopatch enables high-fidelity optical stimulation and recording in cultured neurons. (**a**) Trafficking of Optopatch components in cultured rat hippocampal neurons. Left, CheRiff-EGFP, measured via EGFP fluorescence. Right, QuasAr2, measured via retinal fluorescence. Scale bars, 20 μm (top) and 5 μm (bottom). (**b**) Optical initiation and monitoring of single APs. Blue, illumination; red, whole-cell single-trial unfiltered fluorescence; black, patch-clamp recording. (**c**) Optical mapping of an AP induced via illumination of the soma. Top, filmstrip showing average of $n = 20$ temporally registered APs. Fluorescence is normalized to the mean fluorescence of the dendrite. Images are composites of mean fluorescence (gray) and changes in fluorescence (heat map). Arrow indicates dendritic spine. Scale bar, 5 μm. Bottom, single-trial detection of back-propagating APs in a single dendritic spine. Scale bar, 1 μm. Top traces, ten single-trial recordings from the spine (red) and their average (blue). Bottom traces, ten single-trial recordings from the parent dendrite. Blue bars indicate optical stimulation. (**d**) Synaptic transmission. Optical stimulation of one soma (highlighted in blue) and optical recordings in the stimulated cell (i) and neighboring cell (ii) with and without synaptic blockers. ROI, region of interest. Blue bars indicate optical stimulation. (**e**) Subframe interpolation of AP propagation in a neuron expressing Optopatch1 (**Supplementary Video 4**). Scale bar, 50 μm. Bottom right, immunostaining of the same cell with anti-EGFP and anti-ankyrinG (AnkG). Scale bar, 25 μm. Arrows indicate the site of AP initiation, the distal end of the axon initial segment (AIS). (**f**) Parallel optical recording under increasingly strong 0.5-s optical step stimuli. Asterisk indicates a cell that showed periodic bursts of three or four APs under weak stimulation. Scale bar, 500 μm. Image is of EGFP fluorescence. Data in **a**,**c**,**f** acquired on an sCMOS detector; data in **b**,**d**,**e** acquired on an EMCCD.

device (DMD) to pattern the blue CheRiff excitation[26] and wide-field red illumination to monitor voltage throughout the field of view (Online Methods).

We probed synaptic transmission by optically stimulating the soma of single cells and optically monitoring electrical responses in neighboring cells. Optically induced single APs in the presynaptic cell led to fluorescence transients indicative of excitatory postsynaptic potentials, as well as to occasional failures of synaptic transmission, in the postsynaptic cell (**Fig. 3d**). The mean interval between the peak of the AP in the upstream cell and the onset of the optically detected excitatory postsynaptic potential in the downstream cell was <2 ms, indicating a monosynaptic connection[27]. Addition of synaptic blockers (10 μM NBQX, 20 μM gabazine, 25 μM AP-V) quieted the fluorescence response in the postsynaptic cell without perturbing presynaptic activity. Validation measurements with patch-clamp recordings showed millivolt-level correspondence of optically and electrically recorded postsynaptic potentials as well as inhibition of these signal by synaptic blockers (**Supplementary Fig. 12**).

**Probing action potential propagation**

We next sought to apply the extremely fast response of Optopatch1 (containing QuasAr1) to probe the microsecond-timescale dynamics of AP initiation and propagation within a single cell. We used the DMD to target optical stimulation to either a dendrite or the soma and recorded the fluorescence dynamics at a 1-kHz frame rate. To improve the SNR we averaged 100–400 temporally registered optically induced APs. These mean-AP movies showed spreading of the subthreshold voltage outward from the stimulated region followed by a sudden spike in cell-wide fluorescence that peaked within two frames (**Supplementary Video 3**). Thus the native 1-kHz frame rate was insufficient to resolve the details of AP propagation.

To probe microsecond-level dynamics, we adapted the subframe interpolation approach of Foust *et al.*[28] and Popovic *et al.*[29] (**Supplementary Fig. 13** and **Supplementary Software**). By interpolating a smoothly varying spline to the fluorescence intensity time trace at each pixel, we inferred the timing with which the fluorescence crossed a user-selected threshold (for example, 50% maximum deviation) with a precision better than the exposure time of the camera. Mean deviation between optically inferred and electrically recorded AP timing at the soma was 40–70 μs (**Supplementary Fig. 13**). We then constructed a higher time-resolution movie highlighting each pixel at the subframe time of its wavefront crossing. This interpolation technique does not rely on an assumed AP waveform, nor does it assume wavelike

propagation; it is compatible with APs that change shape within or between cells.

The visually striking propagation movies clearly showed AP initiation 30–50 µm from the soma in a single thin neurite, presumed to be the axon, in $n = 8$ of 8 measured cells (**Supplementary Fig. 13e** and **Supplementary Videos 4–6**) regardless of stimulus location. The AP then propagated down the putative axon and back into the soma and dendrites. Latencies between AP initiation and arrival in the soma were $320 \pm 220$ µs ($n = 8$ cells, mean $\pm$ s.d.).

After acquiring Optopatch data, we fixed the cells and stained for ankyrinG, a marker of the axon initial segment (AIS; **Fig. 3e**). The optically detected zones of AP initiation coincided with the distal end of the AIS, which is consistent with previous experiments using voltage-sensitive dyes[30]. Thus Optopatch can resolve functionally significant subcellular and microsecond-timescale details of AP dynamics.

### Parallel measurements in neuronal cultures

To achieve high-throughput functional characterization in neurons, one would like to apply the technique to many cells in parallel. We constructed a low-magnification, high-speed microscope (**Supplementary Fig. 14** and Online Methods) that robustly reported APs and subthreshold dynamics in up to ~50 cells simultaneously (**Supplementary Video 7**). We used a DMD to pattern the blue illumination for targeted CheRiff excitation in user-selected regions. Optical stimulation of a segment of a synaptically connected culture induced network activity that manifested as APs and subthreshold dynamics in the cells not directly stimulated (**Supplementary Fig. 15**).

We developed an all-optical protocol to measure neuronal excitability. Synaptic blockers were added to suppress network activity. Cells were stimulated with pulses of blue light (500 ms at 6-s intervals) of increasing intensity (0–14 mW/cm$^2$) while firing patterns were recorded under continuous red illumination (100 W/cm$^2$). In wide-field measurements on $n = 169$ neurons expressing Optopatch2, we observed several distinct firing patterns, including fast-adapting and slow-adapting spike trains (**Fig. 3f** and **Supplementary Video 8**). Two neurons showed intermittent bursting. The comparatively high throughput of Optopatch measurements enables detection of rare electrophysiological phenotypes that might be missed in a manual patch-clamp measurement on a smaller number of cells.

To test whether high-throughput Optopatch could quantify subtle electrophysiological shifts, we applied the all-optical excitability protocol to a model of homeostatic plasticity of intrinsic excitability (HPIE)[31], in which neurons adapt their excitability to maintain an approximately constant level of activity. Observation of HPIE in culture[32,33] and *in vivo*[34] has traditionally required laborious patch-clamp measurements on many cells.

Neurons expressing Optopatch2 were incubated in tetrodotoxin (TTX, 1 µM) for 48 h and then measured in TTX-free medium in the presence of synaptic blockers[32]. Paired control cultures were incubated without TTX. Cells that had been treated with TTX ($n = 94$) subsequently showed a significantly lower illumination threshold for spiking ($P = 5 \times 10^{-6}$, Mann-Whitney $U$-test), shorter interval between first and second spike ($P < 0.001$) and more total spikes ($P < 0.01$) than control cells ($n = 75$), but only a small change in time from light onset to first spike (**Supplementary Fig. 16**), consistent with previous reports[32]. Total data acquisition time

was less than 1 h, a fraction of the time that would be required for manual measurements.

Although the HPIE measurements showed population-level changes in excitability, a unique promise of Optopatch is the ability to measure the same cell over several days. In 8 of 10 trials, neurons measured with a 1-min Optopatch protocol were identified and rerecorded 48 h later (**Supplementary Fig. 17**). This capability could be useful for studying neuronal maturation or long-term effects of pharmacological, genetic or environmental perturbations.

### Probing excitability in hiPSC-derived neurons

Human-derived neurons show promise as a platform for studying human neurophysiology in health and disease[35]. However, variability arises at multiple levels in this approach[4]. Each patient's genetic background modifies neuronal function, even for nominally monogenic diseases. Additional variability arises between iPSC clones from a single patient, between differentiations and between cells cultured within a single well. Differing degrees of maturation are a particularly large source of cell-to-cell variability within a dish[36]. Furthermore, for disease-modeling efforts, one may wish to test many differentiation protocols or pharmacological perturbations. Together these factors motivate a need for accurate functional characterization with robust statistics. The low throughput and selection bias of manual electrophysiology present a serious bottleneck.

We first assessed whether Optopatch expression perturbed electrophysiology in hiPSC-derived neurons. Cells were transfected with Optopatch2 and cultured on a rat glial monolayer. The *CaMKIIα* promoter genetically targeted the measurement to mature neurons within this highly heterogeneous culture[36]. Patch-clamp measurements on cells transfected with Optopatch2 ($n = 11$) or with GFP ($n = 11$) showed no significant difference in membrane resistance ($P = 0.82$, two-tailed student's $t$-test), membrane capacitance ($P = 0.88$), resting potential ($P = 0.34$) or AP activation threshold ($P = 0.78$) (**Supplementary Fig. 18**). Optically evoked and optically monitored trains of APs showed the expected changes upon addition of ion channel blockers lidocaine and tetraethylamine (**Supplementary Fig. 19**).

We then applied Optopatch to test for HPIE in hiPSC-derived neurons. This subtle form of neural plasticity has not previously been reported in human-derived neurons. hiPSC-derived neurons were incubated in 1 µM TTX for 48 h. Upon return to TTX-free medium, treated cells showed a substantial increase in subsequent optically measured excitability ($n = 31$ cells) relative to controls ($n = 32$ cells) (**Fig. 4a–e**), demonstrating positive HPIE.

We next tested for negative HPIE: conditions that depolarize cells (for example, high KCl) induce a gradual decrease in intrinsic excitability[33]. hiPSC-derived neurons were incubated in 15 mM KCl for 60 h. Upon return to baseline conditions (2.5 mM KCl), treated cells showed a substantial decrease in subsequent optically measured excitability ($n = 28$ cells) relative to controls ($n = 25$ cells) (**Fig. 4f–j**).

Post-measurement immunostaining with anti-human nuclear antigen 1 and anti-GFP antibodies confirmed that all neurons tested were of human origin (**Supplementary Fig. 20**). Validation measurements with manual patch clamp confirmed that the HPIE protocols did not change CheRiff photocurrents (**Supplementary Fig. 21**).
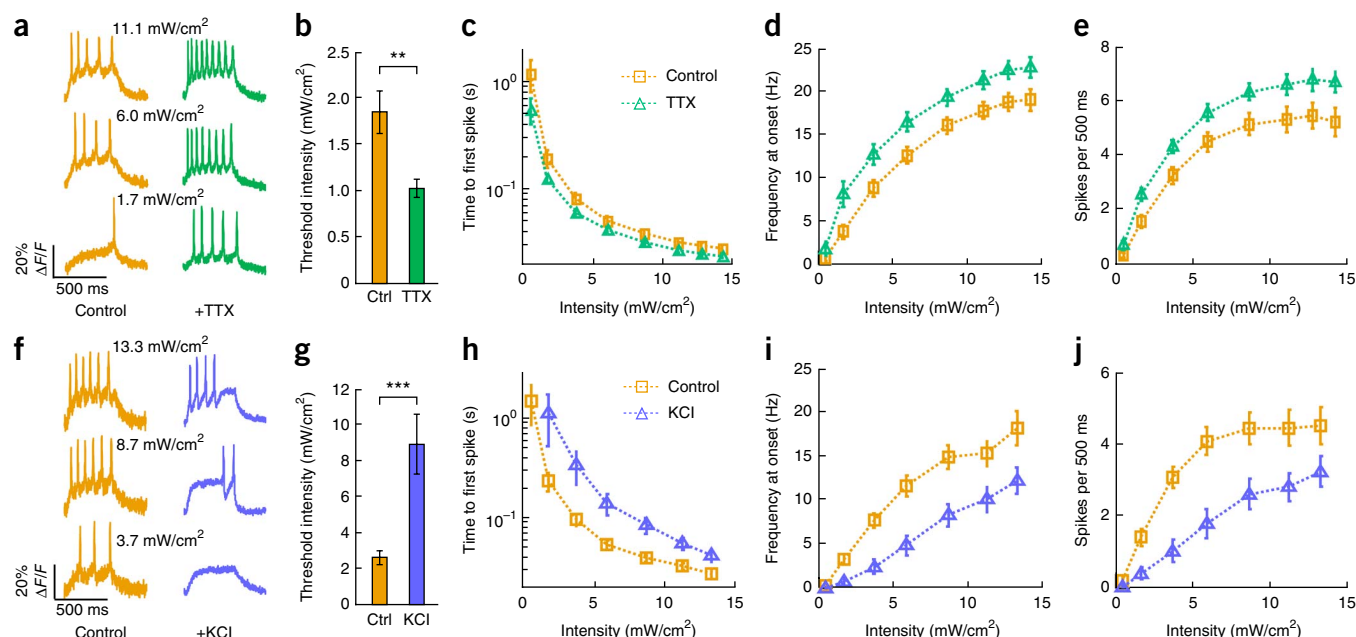
**Figure 4** | Homeostatic plasticity of intrinsic excitability in hiPSC-derived neurons probed via Optopatch2. (**a**–**e**) Positive homeostatic plasticity of intrinsic excitability (HPIE). Data from $n = 32$ control (Ctrl) cells and $n = 31$ TTX-treated cells. (**a**) Representative optical recordings from single neurons after incubation in TTX and matched control cells. (**b**) Threshold stimulation intensity (488 nm) to induce at least one spike in 500 ms. \*\*$P = 0.004$ (Mann-Whitney $U$-test). (**c**) Time from onset of illumination to first spike. (**d**) Spike frequency at onset (inverse time between first and second spike). (**e**) Total spikes per 500-ms stimulus. Curves in **d** and **e** are significantly different from each other ($P < 0.05$ for each stimulation intensity $\geq$1.7 mW/cm$^2$; two-tailed Student's $t$-test or Mann-Whitney $U$-test). (**f**–**j**) Negative HPIE. Data from $n = 25$ control cells and $n = 28$ KCl-treated cells. Panels are the same as **a**–**e**. \*\*\*$P = 7 \times 10^{-6}$ (Mann-Whitney $U$-test). Curves in **h**–**j** are significantly different from each other (**h**, $P < 0.01$ for all stimulus intensities; **i**, $P < 0.05$ for stimulus intensities $\geq$1.7 mW/cm$^2$; **j**, $P < 0.05$ for stimulus intensities $\leq$11.2 mW/cm$^2$; two-tailed Student's $t$-test or Mann-Whitney $U$-test). For all experiments fluorescence was excited at 300 W/cm$^2$ and collected at a 1-kHz frame rate on an EMCCD. Error bars, s.e.m.

These experiments demonstrate that hiPSC-derived neurons undergo bidirectional HPIE and that Optopatch measurements can nonperturbatively report subtle differences in electrophysiology in these cells. High-throughput Optopatch measurements have promise as a powerful means for functional characterization of neuronal populations in hiPSC-based disease modeling efforts.

## Imaging in organotypic slice culture

Voltage imaging with GEVIs in intact tissue would enable functional mapping of subcellular and circuit-level signal processing. Application of GEVIs to recording of APs in mammalian brain tissue has been limited by the low voltage sensitivity and slow response of existing indicators[37,38]. No GEVI has been shown to report single-trial APs in tissue with high fidelity.

We expressed Optopatch2 in organotypic brain slice using biolistic gene delivery. Neurons that had taken up the gene were clearly visible via fluorescence of EGFP (indicating CheRiff) and QuasAr2 under wide-field epifluorescence imaging (20× numerical aperture (NA) 1.0 water-immersion objective) (**Fig. 5a**). Upon illumination with pulses of blue light (10 ms, repeated at 5 Hz, 7.5 mW/cm$^2$), the fluorescence under red excitation (1,200 W/cm$^2$ nominal incident intensity, not corrected for light scatter) showed clearly resolved single-trial APs in the soma (**Fig. 5b**)
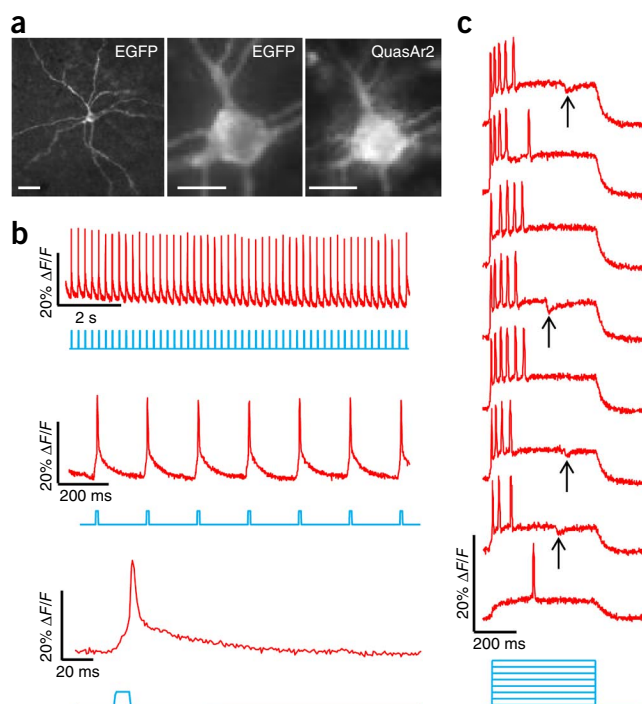


**Figure 5** | Optopatch2 in organotypic brain slice. (**a**) EGFP fluorescence, indicating CheRiff distribution (left and center), and QuasAr2 fluorescence (right). Scale bars, from left to right: 50 μm, 20 μm, 20 μm. (**b**) Single-trial optical recordings of APs initiated by pulses of blue illumination (10 ms, 7.5 mW/cm$^2$). Signal represents whole-soma fluorescence without photobleaching correction or background subtraction. (**c**) Responses triggered by steps of blue illumination (500 ms, 1–10 mW/cm$^2$). Arrows indicate inhibitory potentials. For **b** and **c**, red illumination was 1,200 W/cm$^2$ nominal incident intensity, not corrected for light scatter. Fluorescence collected at a frame rate of 1 kHz on an EMCCD camera.

and in dendrites (**Supplementary Fig. 22**). These traces represent raw fluorescence without background subtraction or correction for photobleaching.

We performed Optopatch measurements on $n = 7$ separately prepared organotypic brain slices (**Supplementary Fig. 23**). AP amplitudes ranged from $\Delta F/F$ of 7.2% to 26.1% (mean 15.9%, $n = 7$ cells), calculated without subtraction of background autofluorescence. Whole cell-body fluorescence reported APs with SNRs ranging from 7.8 to 65.6 (mean 31.9) in a 1 kHz bandwidth. At lower red excitation intensity (400 W/cm² nominal incident intensity, not corrected for light scatter), whole cell-body fluorescence reported APs with SNRs ranging from 7.2 to 35.7 (mean 16.5) in a 1-kHz bandwidth.

We further tested the response of neurons in tissue to extended pulses of blue illumination (0.5 s, 1–10 mW/cm²). This stimulus elicited a variety of firing patterns, including single spikes, bursts (**Fig. 5c**) and sustained activation (**Supplementary Fig. 23**). Optically induced spike trains were often interrupted by hyperpolarizing fluorescence transients, which we provisionally ascribe to inhibitory feedback in the local microcircuit. We did not observe these inhibitory potentials in the absence of optical stimulation. These results demonstrate the feasibility of optically measuring single-cell, single-trial AP waveforms, excitability and subthreshold dynamics in tissue with high SNR.

Finally, we compared Optopatch to ArcLight in organotypic slice preparations (**Supplementary Fig. 23**). Under manual patch-clamp stimulation, ArcLight fluorescence resolved single APs with a mean value of $\Delta F/F = -1.5\% \pm 0.4\%$ and an SNR of $7.1 \pm 2.8$ ($n = 6$ cells) (excitation at 488 nm, 50 W/cm²). The ArcLight fluorescence transients had a mean width (at 70% maximum deviation) of $21.5 \pm 3.0$ ms. Thus QuasAr2 reports APs in tissue with greater sensitivity, higher SNR and better temporal resolution than ArcLight.

## DISCUSSION

The combination of an improved reporter and improved actuator in the Optopatch constructs facilitates rapid, non-invasive characterization of genetically defined cells across spatial scales from micrometers to millimeters and across temporal scales from microseconds to days. Optopatch has not yet been implemented with real-time feedback on the illumination, so it is not suited for voltage-clamp experiments. Nonetheless, with the assistance of computational modeling, open-loop voltage measurements can probe ionic conductances and membrane electrical properties[39,40]. Absolute voltage measurements with GEVIs are challenging owing to variations in expression level and membrane trafficking. A recent report demonstrated measurements of absolute voltage through its effect on photocycle dynamics in an archaerhodopsin mutant[41]. A similar strategy may apply to the QuasArs.

Our discovery of homeostatic plasticity in intrinsic excitability of hiPSC-derived neurons serves as a paradigm for other Optopatch assays of neuronal excitability. Such assays may probe cell-autonomous functional phenotypes in hiPSC-based models of diseases such as amyotrophic lateral sclerosis[42], epilepsy[43] and Parkinson's disease[44]. Other neurodevelopmental and neuropsychiatric diseases arise primarily through synaptic dysfunction. These include Rett syndrome[45], fragile X[46], and Phelan-McDermid syndrome[36]. Development of robust assays of synaptic function

will probably benefit from incorporation of cell patterning techniques to control the type and location of synaptic connections. A merit of optical electrophysiology for disease modeling and drug screening is that it does not require mechanical access; thus it is compatible with microfluidic compound delivery and high-throughput experimental formats. Optopatch measurements preserve the sterility of the sample and the integrity of the cell membrane and thus are compatible with studies of long-term responses to chronic pharmacological perturbations.

We demonstrated that Optopatch functions in intact mammalian tissue. With extension to multiple genetically specified cells, Optopatch measurements in tissue may provide a useful tool for functional circuit mapping[2]. With improved optical sectioning capability, subcellular Optopatch measurements could enable inference of electrophysiological parameters in multicompartment neural models of single-cell information processing.

For applications *in vivo*, the new QuasAr reporters are likely to be appropriate for measurements on a few cells or small networks. The required laser power scales with the field of view, so tissue heating may be a concern for fields of view >~200 μm on a side. Applications to larger circuits will likely benefit from further improvements to the indicator, primarily increased brightness, and exploration of two-photon excitability or other contrast modalities. Small transparent organisms, for example, zebrafish and *Caenorhabditis elegans*, are probable early targets as most illumination passes through their bodies without depositing heat.

## METHODS

Methods and any associated references are available in the online version of the paper.

**Accession codes.** Plasmids are available on Addgene. DRH229: FCK-QuasAr1-mO2, 51629; DRH334: FCK-QuasAr2-mO2, 51692; DRH313: FCK-CheRiff-eGFP, 51693; DRH296: FCK-Optopatch2 , 51694; DRH335: FCK-Optopatch1, 51695; DRH322: AAV-CaMKIIa-QuasAr2-mO2, 51696; DRH337: AAV-hsyn-CheRiff-eGFP, 51697.

*Note: Any Supplementary Information and Source Data files are available in the online version of the paper.*

**AUTHOR CONTRIBUTIONS**
D.R.H. designed the Optopatch construct and system. Y.Z. and D.R.H. engineered the QuasArs. D.R.H., N.K. and Y.K.C. engineered CheRiff. D.R.H.

1. Peron, S. & Svoboda, K. From cudgel to scalpel: toward precise neural control with optogenetics. *Nat. Methods* **8**, 30–34 (2011).
2. Petreanu, L., Mao, T., Sternson, S.M. & Svoboda, K. The subcellular organization of neocortical excitatory connections. *Nature* **457**, 1142–1145 (2009).
3. Scanziani, M. & Hausser, M. Electrophysiology in the age of light. *Nature* **461**, 930–939 (2009).
4. Boulting, G.L. *et al.* A functionally characterized test set of human induced pluripotent stem cells. *Nat. Biotechnol.* **29**, 279–286 (2011).
5. Furuta, T. *et al.* Brominated 7-hydroxycoumarin-4-ylmethyls: photolabile protecting groups with biologically useful cross-sections for two photon photolysis. *Proc. Natl. Acad. Sci. USA* **96**, 1193–1200 (1999).
6. Kramer, R.H., Fortin, D.L. & Trauner, D. New photochemical tools for controlling neuronal activity. *Curr. Opin. Neurobiol.* **19**, 544–552 (2009).
7. Boyden, E.S., Zhang, F., Bamberg, E., Nagel, G. & Deisseroth, K. Millisecond-timescale, genetically targeted optical control of neural activity. *Nat. Neurosci.* **8**, 1263–1268 (2005).
8. Looger, L.L. & Griesbeck, O. Genetically encoded neural activity indicators. *Curr. Opin. Neurobiol.* **22**, 18–23 (2012).
9. Miller, E.W. *et al.* Optically monitoring voltage in neurons by photo-induced electron transfer through molecular wires. *Proc. Natl. Acad. Sci. USA* **109**, 2114–2119 (2012).
10. Yan, P. *et al.* Palette of fluorinated voltage-sensitive hemicyanine dyes. *Proc. Natl. Acad. Sci. USA* **109**, 20443–20448 (2012).
11. Vogt, K.E., Gerharz, S., Graham, J. & Canepari, M. Combining membrane potential imaging with l-glutamate or GABA photorelease. *PLoS ONE* **6**, e24911 (2011).
12. Tsuda, S. *et al.* Probing the function of neuronal populations: combining micromirror-based optogenetic photostimulation with voltage-sensitive dye imaging. *Neurosci. Res.* **75**, 76–81 (2013).
13. Lim, D.H. *et al. In vivo* large-scale cortical mapping using channelrhodopsin-2 stimulation in transgenic mice reveals asymmetric and reciprocal relationships between cortical areas. *Front. Neural Circuits* **6**, 11 (2012).
14. Gong, Y., Li, J.Z. & Schnitzer, M.J. Enhanced archaerhodopsin fluorescent protein voltage indicators. *PLoS ONE* **8**, e66959 (2013).
15. Klapoetke, N.C. *et al.* Independent optical excitation of distinct neural populations. *Nat. Methods* **11**, 338–346 (2014).
16. Jin, L. *et al.* Single action potentials and subthreshold electrical events imaged in neurons with a fluorescent protein voltage probe. *Neuron* **75**, 779–785 (2012).
17. Kralj, J.M., Douglass, A.D., Hochbaum, D.R., Maclaurin, D. & Cohen, A.E. Optical recording of action potentials in mammalian neurons using a microbial rhodopsin. *Nat. Methods* **9**, 90–95 (2012).
18. Maclaurin, D., Venkatachalam, V., Lee, H. & Cohen, A.E. Mechanism of voltage-sensitive fluorescence in a microbial rhodopsin. *Proc. Natl. Acad. Sci. USA* **110**, 5939–5944 (2013).
19. Sakai, R., Repunte-Canonigo, V., Raj, C.D. & Knöpfel, T. Design and characterization of a DNA-encoded, voltage-sensitive fluorescent protein. *Eur. J. Neurosci.* **13**, 2314–2318 (2001).
20. Bean, B.P. The action potential in mammalian central neurons. *Nat. Rev. Neurosci.* **8**, 451–465 (2007).
21. Schoenenberger, P., Grunditz, Å., Rose, T. & Oertner, T.G. Optimizing the spatial resolution of Channelrhodopsin-2 activation. *Brain Cell Biol.* **36**, 119–127 (2008).
22. Johnson, M.T.J. *et al.* Evaluating methods for isolating total RNA and predicting the success of sequencing phylogenetically diverse plant transcriptomes. *PLoS ONE* **7**, e50226 (2012).
23. Melkonian, M. & Preisig, H.R. A light and electron microscopic study of *Scherffelia dubia*, a new member of the scaly green flagellates (Prasinophyceae). *Nord. J. Bot.* **6**, 235–256 (1986).
24. Mattis, J. *et al.* Principles for applying optogenetic tools derived from direct comparative analysis of microbial opsins. *Nat. Methods* **9**, 159–172 (2012).
25. Lin, J.Y., Lin, M.Z., Steinbach, P. & Tsien, R.Y. Characterization of engineered channelrhodopsin variants with improved properties and kinetics. *Biophys. J.* **96**, 1803–1814 (2009).
26. Takahashi, H. *et al.* Light-addressed single-neuron stimulation in dissociated neuronal cultures with sparse expression of ChR2. *Biosystems* **107**, 106–112 (2012).
27. Fitzsimonds, R.M., Song, H.-j. & Poo, M.-m. Propagation of activity-dependent synaptic depression in simple neural networks. *Nature* **388**, 439–448 (1997).
28. Foust, A., Popovic, M., Zecevic, D. & McCormick, D.A. Action potentials initiate in the axon initial segment and propagate through axon collaterals reliably in cerebellar Purkinje neurons. *J. Neurosci.* **30**, 6891–6902 (2010).
29. Popovic, M.A., Foust, A.J., McCormick, D.A. & Zecevic, D. The spatio-temporal characteristics of action potential initiation in layer 5 pyramidal neurons: a voltage imaging study. *J. Physiol.* (*Lond.*) **589**, 4167–4187 (2011).
30. Kole, M.H. & Stuart, G.J. Signal processing in the axon initial segment. *Neuron* **73**, 235–247 (2012).
31. Turrigiano, G., Abbott, L. & Marder, E. Activity-dependent changes in the intrinsic properties of cultured neurons. *Science* **264**, 974–977 (1994).
32. Desai, N.S., Rutherford, L.C. & Turrigiano, G.G. Plasticity in the intrinsic excitability of cortical pyramidal neurons. *Nat. Neurosci.* **2**, 515–520 (1999).
33. Grubb, M.S. & Burrone, J. Activity-dependent relocation of the axon initial segment fine-tunes neuronal excitability. *Nature* **465**, 1070–1074 (2010).
34. Lambo, M.E. & Turrigiano, G.G. Synaptic and intrinsic homeostatic mechanisms cooperate to increase L2/3 pyramidal neuron excitability during a late phase of critical period plasticity. *J. Neurosci.* **33**, 8810–8819 (2013).
35. Trounson, A., Shepard, K.A. & DeWitt, N.D. Human disease modeling with induced pluripotent stem cells. *Curr. Opin. Genet. Dev.* **22**, 509–516 (2012).
36. Shcheglovitov, A. *et al.* SHANK3 and IGF1 restore synaptic deficits in neurons from 22q13 deletion syndrome patients. *Nature* **503**, 267–271 (2013).
37. Akemann, W. *et al.* Imaging neural circuit dynamics with a voltage-sensitive fluorescent protein. *J. Neurophysiol.* **108**, 2323–2337 (2012).
38. Cao, G. *et al.* genetically targeted optical electrophysiology in intact neural circuits. *Cell* **154**, 904–913 (2013).
39. Huys, Q.J., Ahrens, M.B. & Paninski, L. Efficient estimation of detailed single-neuron models. *J. Neurophysiol.* **96**, 872–890 (2006).
40. Williams, J.C. *et al.* Computational optogenetics: empirically-derived voltage-and light-sensitive channelrhodopsin-2 model. *PLoS Comput. Biol.* **9**, e1003220 (2013).
41. Hou, J.H., Venkatachalam, V. & Cohen, A.E. Temporal dynamics of microbial rhodopsin fluorescence reports absolute membrane voltage. *Biophys. J.* **106**, 639–648 (2014).
42. Wainger, B.J. *et al.* Intrinsic membrane hyperexcitability of amyotrophic lateral sclerosis patient-derived motor neurons. *Cell Rep.* **7**, 1–11 (2014).
43. Higurashi, N. *et al.* A human Dravet syndrome model from patient induced pluripotent stem cells. *Mol. Brain* **6**, 19 (2013).
44. Badger, J.L., Cordero-Llana, O., Hartfield, E.M. & Wade-Martins, R. Parkinson's disease in a dish–using stem cells as a molecular tool. *Neuropharmacology* **76**, 88–96 (2014).
45. Marchetto, M.C. *et al.* A model for neural development and treatment of Rett syndrome using human induced pluripotent stem cells. *Cell* **143**, 527–539 (2010).
46. Auerbach, B.D., Osterweil, E.K. & Bear, M.F. Mutations causing syndromic autism define an axis of synaptic pathophysiology. *Nature* **480**, 63–68 (2011).

## ONLINE METHODS

**Engineering of Arch.** We adopted a hierarchical approach to screening that prioritized brightness over multiple secondary selection criteria. The brightness screen was conducted by examining the fluorescence of large libraries of variants expressed in bacterial colonies. Subsequent screens for trafficking, speed and voltage sensitivity were performed in HeLa cells subjected to field stimulation and induced transmembrane voltages, and then in HEK cells with patch clamp.

*Molecular biology procedure.* Synthetic DNA oligonucleotides used for cloning and library construction were purchased from Integrated DNA Technologies (primers used for directed evolution of QuasArs are in **Supplementary Table 6**). *Pfu* polymerase (Fermentas) or AccuPrime *Pfx* SuperMix (Invitrogen) was used for high-fidelity nonmutagenic PCR amplifications in the buffer supplied by the respective manufacturer. *Taq* polymerase (New England BioLabs) in the presence of 0.1 mM $MnCl_2$, 7 mM $MgCl_2$, 0.2 mM each of dGTP and dATP, and 1.0 mM each of dCTP and dTTP was used for error-prone PCR. PCR products and products of restriction digests were routinely purified using preparative agarose gel electrophoresis followed by DNA isolation using the GeneJET gel extraction kit (Fermentas). Restriction endonucleases were purchased from Fermentas and used according to the manufacturer's recommended protocol. Ligations were performed using T4 ligase (Invitrogen) or Gibson Assembly (New England BioLabs). Small-scale isolation of plasmid DNA was performed by GeneJET miniprep kit (Fermentas). The cDNA sequences for all Arch variants and fusion constructs were confirmed by dye terminator cycle sequencing using the BigDye Terminator Cycle Sequencing kit (Applied Biosystems). Site-directed mutagenesis and randomization of targeted codons was performed with either the QuikChange Lightning Single or Multi kit (Agilent Technologies).

*Construction of Arch mutant libraries.* A library of >$10^4$ mutants was generated by error-prone PCR of the gene encoding Arch D95N. These variants were then joined with the gene encoding mOrange2 by a two-part overlap extension PCR. The 5′ piece used in the overlap extension was prepared by error-prone PCR of Arch D95N as template with a mixture of the forward primer (Fw_XbaI_Arch) and reverse primer (RV_Arch). Primer Fw_XbaI_Arch contains an XbaI site, and primer RV_Arch contains an overlap region with primer FW_Arch_FP. The 3′ piece for use in the overlap extension was prepared by high-fidelity PCR amplification of mOrange2 using a forward primer (FW_Arch_FP) and a reverse primer (RV_HindIII_FP). Primer RV_HindIII_FP contains a stop codon and a HindIII site. The full-length Arch-mOrange2 gene library was assembled by overlap extension PCR using an equimolar mixture of primers Fw_XbaI_Arch and RV_HindIII_FP together with a mixture of the 5′ and 3′ PCR fragments described above (50 ng each) as the template. In later rounds of directed evolution, error-prone PCR and StEP PCR DNA shuffling[47] were both used for construction of Arch-mOrange2 gene libraries.

The full-length PCR product (approximately 1,500 bp) was purified by agarose gel electrophoresis, doubly digested, and ligated between the XbaI and HindIII sites of a modified pBAD vector that was generated by deleting the ETorA tag between the NcoI and XbaI sites of the pTorPE vector[48] using Quikchange Lightning kit.

Following ligation, electrocompetent *E. coli* strain DH10B was transformed with the library of gene variants and cultured overnight at 37 °C on 10-cm Petri dishes of LB-agar supplemented with 100 µL of 4 mM retinal (Sigma), 100 µg/mL ampicillin (Sigma) and up to 0.0020% (wt/vol) L-arabinose (Alfa Aesar). The retinal solution was added on the surface of LB-agar plates evenly and air dried before plating the cell suspension. At concentrations of L-arabinose higher than 0.0020% (wt/vol) we observed abnormal colony morphologies and reduced fluorescent brightness, presumably owing to cytotoxicity caused by overexpression.

*Screening of Arch mutants in E. coli.* The imaging system used for library screening has previously been described in detail[49]. We screened 10,000–20,000 colonies (10–20 plates of bacterial colonies) per round of random mutagenesis. For libraries generated by randomization of one or more codons, we screened approximately threefold more colonies than the expected library diversity (for example, 3,000 colonies for a 1,000-member library).

We acquired two images of colonies using filter sets for mOrange2 (exc. 540–580 nm, em. 600–660 nm) and Arch (exc. 604–640 nm and em. 660–700 nm). An image of the ratio of Arch:mOrange2 fluorescence was calculated, and the colonies with the top 0.01–0.1% highest ratios were manually picked. Picked clones were individually cultured in 2 mL liquid LB medium (200 µg/mL ampicillin) shaken (250 r.p.m.) overnight at 37 °C.

Protein expression was induced by adding 2 mL of liquid LB medium containing 120 µM retinal, 200 µg/mL ampicillin and 0.2% L-arabinose to the overnight culture, followed by incubation at 37 °C for 3 h. The cell pellets were collected by centrifugation, washed and resuspended in buffered M9 salt solution containing 7 g/L $Na_2HPO_4$, 3 g/L $KH_2PO_4$, 0.5 g/L NaCl and 1 g/L $NH_4Cl$. The suspension was then diluted fivefold before acquisition of its fluorescence spectrum in a Safire 2 fluorescence microplate reader (Tecan).

The emission profiles of each variant under excitation at 525 nm and 600 nm were acquired and normalized by the absorbance at 600 nm. The cell pellets of the three variants with the highest ratios of Arch to mOrange2 and the two variants with the brightest absolute Arch fluorescence were treated for plasmid DNA extraction, and the pooled genes were used as templates for construction of gene libraries in the next round of directed evolution.

After five iterations we arrived at a nonpumping variant of Arch with five mutations relative to wild type (P60S, T80S, D95N, D106Y and F161V) and substantially improved brightness under excitation with low illumination intensity.

An additional round of screening was conducted in an effort to improve the membrane trafficking of this nonpumping variant. The C-terminal sequence of Arch ("VSAADRPVVA") was replaced with "XXM," where X stands for randomized residues, using a Quikchange procedure. Variants that exhibited strong Arch fluorescence were picked and then assessed in HEK cells for improved membrane trafficking. This procedure led to a new variant with the C-terminal sequence "TLM." This variant, designated Arch 3.5, was used as the template for subsequent efforts to address the secondary selection criteria.

*Random mutagenesis at positions Asp95 and Asp106.* We next focused on tuning other properties of Arch including voltage sensitivity, response kinetics, membrane trafficking and the undesirable dependence of brightness on illumination intensity. Positions Asp95 and Asp106 of Arch are structurally aligned with positions Asp85 and Asp96 of bacteriorhodopsin and have been reported to play key roles in proton translocation during the photocycle[50,51]. The voltage-sensing mechanism of Arch is probably due to electric

field–dependent protonation of the retinal Schiff base[17,52], so we reasoned that perturbations of the proton translocation network around the Schiff base could potentially affect the voltage sensitivity, response kinetics or complex photophysics[18].

We constructed libraries in which Asp95 and Asp106 were randomized to a subset of all possible amino acid substitutions. First, we randomized position 95 using codon HVS (where H = A, C or T; V = A, C or G; S = C or G), which encodes for all amino acids except Ala, Gly, Asp, Glu and Val. This library was screened by fluorescence imaging of *E. coli* colonies. Variants that retained a high ratio of Arch-to-mOrange2 fluorescence were picked and expressed in HeLa cells for screening via induced transmembrane voltage (see below).

The mutation N95H emerged as the best from the first round of screening in HeLa cells. We then constructed a second library by randomizing position 106 to a subset of amino acids with polar or charged side chains (codon NRC, where N = A, C, G or T; R = A or G), and screened these in HeLa cells. The variant with histidine at position 106 proved most promising and was designated QuasAr1.

*Solubilization and spectroscopic characterization of QuasAr1 and QuasAr2. E. coli* expressing QuasAr1 and QuasAr2 were grown in 12 mL liquid LB medium with 200 µg/mL ampicillin overnight. The next day, 12 mL of liquid LB medium containing 50 µM retinal, 200 µg/mL ampicillin and 0.1% arabinose was added into the overnight culture, followed by additional incubation at 37 °C for 4 h. The cell pellets were collected by centrifugation and lysed by suspension in B-PER solution (Pierce). The cytoplasmic fraction was discarded after centrifugation, and the colored insoluble fraction was resuspended in phosphate buffered saline (PBS) containing 1.5% *n*-dodecyl-β-D-maltopyranoside (Affymetrix). The suspension was homogenized by an ultrasonic homogenizer and centrifuged ($17,000g$ for 15 min, 4 °C). The solubilized protein in the supernatant was used for *in vitro* spectroscopic characterization.

Absorption spectra were recorded on a DU-800 UV-visible spectrophotometer (Beckman) and fluorescence spectra were recorded on a Safire2 plate reader (Tecan). Cy5 carboxylic acid (Cyandye) was used as the reference for quantum yield measurement. Quantum yield measurements were performed on a series of dilutions of each protein solution and standard, with absorbance values ranging from 0.01 to 0.05 at 600 nm. The fluorescence emission spectra of each dilution were recorded with excitation at 600 nm, and the total fluorescence intensities were obtained by integration. Integrated fluorescence intensity vs. absorbance was plotted for each protein and each standard. Quantum yields, $\Phi$, were determined from the slopes ($S$) of each line using the equation: $\Phi_{protein} = \Phi_{standard} \times (S_{protein}/S_{standard})$.

*Expression vectors for HeLa cells.* To express Arch-mOrange2 variants in HeLa cells, the gene in the pBAD vector was first amplified by PCR using primers Fw_BamHI_Kozak_Arch and RV_FP_ERex_stp_XbaI. This reverse primer encodes the endoplasmic reticulum (ER) export sequence from the inward-rectifier potassium channel Kir2.1 (FCYENE)[53], which has been reported to be effective for improving the membrane trafficking of Arch in mammalian cells[54].

The purified DNA was digested with BamHI and XbaI restriction enzymes and ligated into a purified pcDNA3.1 plasmid that had been digested with the same two enzymes. The ligation reaction was used for transformation of electrocompetent *E. coli* strain DH10B cells. Cells were plated on LB agar supplemented with ampicillin, and individual colonies were picked into 4 mL of LB/ampicillin following overnight incubation at 37 °C. Liquid cultures were shaken at 250 r.p.m. and 37 °C for 12–15 h, and then a small scale isolation of plasmid DNA was performed. Each gene in pcDNA3.1 was fully sequenced using T7_FW, and BGH_RV primers. Plasmids were then used for cell transfection as described below.

*Induced transmembrane voltage (ITV) in HeLa cells.* We coexpressed prospective Arch variants in HeLa cells with the inward rectifier potassium channel Kir2.1. Expression of Kir2.1 lowered the resting potential to approximately −60 mV, close to the resting potential of neurons[55,56]. We reasoned that this effect would center the ITV close to the physiologically relevant range.

HeLa cells were grown to 40–60% confluence on homemade 35-mm glass-bottom dishes or 24-well glass-bottom plates. Cells were transfected with 1 µg of plasmid DNA comprising a 1:1 mixture of Arch variant and Kir2.1, using either 2 µL Turbofect (Thermo Scientific) or 2 µL Lipofectamine 2000 (Invitrogen) according to the manufacturer's instructions. After 3 h of incubation, the medium was exchanged to DMEM with 10% FBS. Cells were incubated for an additional 24 h at 37 °C in a $CO_2$ incubator. Immediately before imaging, cells were washed twice with Hanks balanced salt solution (HBSS), and then 1 mL of 20 mM HEPES buffered HBSS was added.

Cell imaging was performed with an inverted Eclipse Ti-E (Nikon) equipped with a Photometrics QuantEM 512SC camera, a 150-W mercury-xenon lamp (Hamamatsu) and a 10-mW 638-nm semiconductor diode laser (56ICS/S2669, Melles Griot CleanBeam) aligned just above the angle for total internal reflection. The filters were 590–650 nm (excitation), 668–738 nm (emission) and 666 nm (dichroic). Movies were acquired at 10 ms per frame. The NIS-Elements Advanced Research software (Nikon) was used for microscope and camera control and data acquisition. A schematic of the setup is shown in **Supplementary Figure 1**.

To probe the response kinetics and voltage sensitivity, we used a pair of parallel platinum electrodes to apply a reproducible electric field across the cell culture and induce transient asymmetries in the membrane voltage[57]. Platinum electrodes with a gap of 0.5 cm were mounted in a custom plastic support. The electrode pair was placed in the imaging dish or well, and voltage pulses from a 6824A 40V/25A DC Power Supply (HP/Agilent) were applied using waveforms generated by a pulse generator PG 58A (Gould Advance Ltd). The typical waveform had square-wave pulses lasting 20 ms and pulse amplitudes from 25 to 35 V. Fluorescence was imaged at a 100-Hz frame rate in $4 \times 4$ binning mode for 10 s. During each voltage pulse, opposite sides of the cell showed opposite fluorescence transients. Typical fluorescence traces are shown in **Supplementary Figure 1**.

Raw fluorescence traces were corrected for background autofluorescence and photobleaching. The average voltage sensitivity ($\Delta F/F_{min}$) and SNR of each Arch variant were compared to those of the best variant of the previous generation, and only the variants with equal or improved performance were chosen as templates for the next round of screening.

*Expression vectors for HEK cells and neurons.* To enable more accurate electrophysiological characterization via patch clamp

in HEK cells and primary neuron cultures, we cloned QuasAr1 into the BamHI/EcoRI sites of lentivirus vector FCK-Arch-GFP (Addgene: 22217). This vector contains a *CaMKIIα* promoter and a woodchuck hepatitis virus post-transcriptional regulatory element (WPRE) after the 3′ end of the open reading frame. The Arch cDNA was generated by PCR using forward primer FW_BamHI_Kozak_Arch_ValSer and overlapping reverse primers RV_FP_TS and RV_TS_ERex_ stp_EcoRI. These reverse primers introduce a trafficking signal (TS) motif and ER export signal peptide sequence at the C terminus of the protein.

*Simultaneous electrophysiology and fluorescence in HEK cells.* HEK293T cells (ATCC CRL-11268) were cultured and transfected following standard protocols[17]. Cells tested negative for mycoplasma. Briefly, HEK293T cells were grown at 37 °C, 5% $CO_2$, in DMEM supplemented with 10% FBS and penicillin-streptomycin. 400 ng of plasmid DNA was transfected using Transit 293T (Mirus) following the manufacturer's instructions and assayed 48 h later. The day before recording, cells were replated onto glass-bottom dishes (In Vitro Scientific) at a density of ~10,000 cells/cm$^2$.

Cells were supplemented with retinal by diluting stock retinal solutions (40 mM, DMSO) in growth medium to a final concentration of 5 μM and then returning the cells to the incubator for 0.5–1 h. All imaging and electrophysiology were performed in Tyrode's medium (containing, in mM: 125 NaCl, 2.5 KCl, 3 CaCl$_2$, 1 MgCl$_2$, 10 HEPES, 30 glucose, pH 7.3, and adjusted to 305–310 mOsm with sucrose). A gap-junction blocker, 2-aminoethoxydiphenyl borate (50 μM, Sigma), was added to eliminate electrical coupling between cells.

Filamented glass micropipettes (WPI) were pulled to a tip resistance of 5–10 MΩ and filled with internal solution containing 125 mM potassium gluconate, 8 mM NaCl, 0.6 mM MgCl$_2$, 0.1 mM CaCl$_2$, 1 mM EGTA, 10 mM HEPES, 4 mM Mg-ATP, 0.4 mM Na-GTP (pH 7.3), adjusted to 295 mOsm with sucrose. Pipettes were positioned with a Sutter MP285 manipulator. Whole-cell, voltage-clamp and current-clamp recordings were acquired using an Axopatch 700B amplifier (Molecular Devices), filtered at 2 kHz with the internal Bessel filter and digitized with a National Instruments PCIE-6323 acquisition board at 5–10 kHz. Data were acquired from only the HEK cells having reversal potentials between −10 and −40 mV, access resistance <25 MΩ and membrane resistance >0.5 GΩ.

Simultaneous whole-cell patch-clamp recordings and fluorescence recordings were acquired on a home-built, inverted epifluorescence microscope, described previously[17] and described below in "Optopatch measurements." Voltage sensitivity of fluorescence was measured by applying a triangle wave of voltage between −100 mV and +50 mV at a slew rate of 25 mV/s. For step-response measurements, voltage-clamp electronics were compensated 90–95%.

We examined variants of QuasAr1 with mutations at position 95 (Asn, Cys, Gln, His and Tyr) and position 106 (Arg, Asp, Asn, Cys, Glu, His, Lys and Tyr). These experiments confirmed that histidine at position 106 provided the best combination of improved voltage sensitivity and fast kinetics. Mutants with Gln, Cys or Asn at position 95 exhibited better voltage sensitivity than QuasAr1 while retaining fast kinetics. We designated the H95Q mutant QuasAr2.

*Analysis of mutations in QuasAr1 and QuasAr2.* We developed a structural model of QuasAr1 (**Supplementary Fig. 2**) based on

homologous protein Arch-2 (PDB: 2EI4, ref. 58). Mutations T80S and F161V are located in the periphery of the protein, whereas P60S is close to the Schiff base of the retinal chromophore. Given their location, we suspect that the T80S and F161V substitutions are unlikely to have a direct impact on the photophysical properties of the protein, and are more likely to have a role in improving the folding efficiency. In contrast, the close proximity of the P60S substitution to the Schiff base suggests that this mutation has a more direct influence on the photophysical properties.

We compared the Arch double mutants Arch(D95H, D106H) (termed "HH") and Arch(D95Q, D106H) (termed "QH") to the corresponding QuasAr1 and QuasAr2 mutants do determine whether the mutations in the proton-transport chain were sufficient to induce the improved sensor performance. QuasAr1 and QuasAr2 were both substantially brighter than the corresponding double mutants (**Supplementary Fig. 3**). Furthermore, the voltage sensitivities of the HH, QH, QuasAr1 and wild-type protein were comparable, and less than the sensitivity of QuasAr2. The QuasArs were faster than their corresponding Arch double mutants. Thus one or more of the three mutations outside the proton transport chain (P60S, T80S, F161V) play an important role in the brightness, sensitivity and speed of the QuasAr mutants.

The constructs described in this paper are available on Addgene, as follows. Addgene ID is listed, followed by the plasmid name and experimental purpose. 51629, DRH229: FCK-QuasAr1-mO2, fluorescent reporter for membrane voltage with improved brightness; 51692, DRH334: FCK-QuasAr2-mO2, fluorescent reporter of membrane voltage with improved sensitivity; 51693, DRH313: FCK-CheRiff-eGFP, channelrhodopsin with improved sensitivity and minimal red light photocurrent; 51694, DRH296: FCK-Optopatch2, coexpression plasmid of QuasAr2 and CheRiff for all-optical electrophysiology; 51695, DRH335: FCK-Optopatch1, coexpression plasmid of QuasAr1 and CheRiff for all-optical electrophysiology; 51696, DRH322: AAV-CaMKIIa-QuasAr2-mO2, AAV production of QuasAr2 fluorescent reporter; and 51697, DRH337: AAV-hsyn-CheRiff-eGFP, AAV production of CheRiff channelrhodopsin actuator.

**Engineering of CheRiff.** The gene for *S. dubia* channelrhodopsin (sdChR) was synthesized with mouse codon optimization. This gene was selected from a screen of channelrhodopsins for its blue excitation peak (474 nm) and its large photocurrent relative to that of ChR2. However, the trafficking in neurons was poor (**Supplementary Fig. 8**). Addition of a trafficking sequence from Kir2.1 improved trafficking greatly[54]. Addition of the ER2 export motif did not appear to further improve trafficking, so this motif was not included in the final construct.

The improved membrane trafficking led to large photocurrents in neurons under blue excitation (2,470 ± 170 pA peak, 488 nm, 500 mW/cm$^2$, $n$ = 3 cells) but also led to unacceptably large photocurrents from the red laser used to illuminate the QuasArs (38 ± 4 pA, steady state, 640 nm, 300 W/cm$^2$). Furthermore, the off-time was undesirably slow ($\tau_{off}$ = 26.0 ± 2.9 ms). Directed by experience with mutations in other rhodopsins, we introduced the mutation E154A, which only slightly decreased the peak photocurrent under blue illumination (to 2,030 ± 100 pA, $n$ = 10) but decreased the crosstalk from red illumination (to 10.5 ± 2.8 pA) and shortened $\tau_{off}$ to 16.0 ± 0.8 ms. This variant, termed CheRiff, showed excellent trafficking and neural activation at low illumination intensities.

doi:10.1038/nmeth.3000

The action spectrum of CheRiff was measured in HEK293 cells ($n = 6$ cells) with a monochromator (Till-Photonics Polychrome IV). 10-ms pulses of nearly equal photon fluxes (~$2.5 \times 10^{21}$ photons/s/m$^2$) were used across wavelengths. Small deviations in photon flux between wavelengths were corrected by dividing the recorded opsin response by the measured photon dose. For each cell, wavelengths were swept from blue to -red and red to blue, and the responses were averaged.

**Design of Optopatch.** We used a 2A peptide ribosomal skip sequence as a means to achieve approximately stoichiometric coexpression of the QuasArs and CheRiff. The porcine teschovirus-1 (P2A) sequence performed better than the *Thosea asigna* virus (T2A) sequence. Owing to the greater need for high expression of the voltage indicator than the actuator, we placed the QuasAr gene before the P2A sequence and the CheRiff gene after (**Supplementary Fig. 10**).

In some applications one might wish to use the visible spectrum for other imaging modalities: for example, for a reporter of Ca$^{2+}$ or a GFP expression marker. In such cases, it is inconvenient to have GFP and mOrange2 fused to CheRiff and Arch, respectively. Removal of the EGFP tag from Arch resulted in poor membrane localization in neurons. To maintain the beneficial trafficking properties of the EGFP tag while eliminating the EGFP fluorescence, we mutated the EGFP chromophore from TYG to GGG using site-directed mutagenesis (Agilent). This mutation has been reported to preserve folding of EGFP[59]. We also made versions of Optopatch in which the mOrange2 was mutated to a nonfluorescent form by the mutation TYG to TAG.

Optopatch constructs were incorporated into lentiviral vectors under the *CaMKIIα* promoter, adapted from Addgene plasmid 22217.

**Neuronal culture and gene delivery.** All procedures involving animals were in accordance with the US National Institutes of Health Guide for the care and use of laboratory animals and were approved by the Institutional Animal Care and Use Committees at Harvard and MIT.

*Primary neurons.* Rat glial monolayers were prepared as described previously[60]. Briefly, 10$^6$ dissociated hippocampal cells from P0 rat pups (Sprague Dawley, Tocris)[61] were plated on a 10-cm culture dish in glial medium, GM, composed of 15% FBS (Life), 0.4% (w/v) D-glucose, 1% GlutaMAX (Life), 1% penicillin/streptomycin (Life) in MEM (Life). When the dish reached confluence (1–2 weeks), cells were split using trypsin onto glass-bottomed dishes (In Vitro Scientific, D35-20-1.5-N) coated with poly(D-lysine) and Matrigel (BD Biosciences) at a density of 3,500 cells/cm$^2$. After ~3–6 d, glial monolayers were at or near confluence, and the medium was replaced by GM with 2 µM cytarabine (cytosine-β-arabinofuranoside, Sigma). Dishes were maintained in GM with 2 µM cytarabine until use. Dishes were discarded if microglia or neurons were identified on the monolayers.

Hippocampal neurons from P0 rat pups were dissected and cultured in neurobasal-based medium (NBActiv4, Brainbits) at a density of 30,000–40,000 neurons/cm$^2$ on the preestablished glial monolayers[61]. At 1 day *in vitro* (DIV), cytarabine was added to the neuronal culture medium at a final concentration of 2 µM to inhibit further glial growth[62].

Neurons were transfected on DIV 7 with the QuasArs or Optopatch plasmids via the calcium phosphate transfection method[63]. Measurements on neurons were taken between DIV 13 and 18.

For comparisons between CheRiff, ChR2 H134R and ChIEF, neurons were plated on glass-bottom dishes coated with poly (D-lysine) (Sigma P7205) and Matrigel (BD Biosciences 356234) without preestablished glial monolayers. On DIV 3, cytarabine (2 µM) was added. Cells were transfected on DIV 7 with channelrhodopsin-EGFP fusions, in identical lentiviral plasmids with a *CaMKIIα* promoter. All comparison measurements were taken between DIV 14 and 15 at room temperature (23 °C).

For TTX-induced homeostatic plasticity, primary neurons were transfected via the calcium phosphate method on DIV 7. TTX (1 µM) was added on DIV 16. Excitability was measured on DIV 18 in Tyrode's medium with synaptic blockers (10 µM NBQX, 25 µM AP-V, 20 µM gabazine).

*hiPSC-derived neurons.* Human iPSC–derived iCell neurons were purchased from Cellular Dynamics Inc. Neurons were tested negative for mycoplasma by the manufacturer. Neurons were thawed and resuspended in complete iCell Neuron Maintenance Medium (CM) following manufacturer protocols. Cells were then plated at a density of 125,000 per cm$^2$ on preestablished rat glial monolayers grown on glass-bottomed dishes. Medium was replaced 24 h post plating with CM supplemented with 10 ng/mL BDNF (PeproTech). Thereafter, 50% medium exchanges with CM were done every 5 d.

For TTX-induced homeostatic plasticity, hiPSC-derived neurons were transfected via the calcium phosphate method on DIV 17. TTX (1 µM) was added on DIV 26. Excitability was measured on DIV 28 in Tyrode's medium with synaptic blockers (10 µM NBQX, 25 µM AP-V, 20 µM gabazine).

For KCl-induced homeostatic plasticity, hiPSC-derived neurons were transfected on DIV 10. KCl (15 mM) was added from DIV 18 to DIV 21 (60 h). Excitability was measured on DIV 21 in Tyrode's medium with synaptic blockers (10 µM NBQX, 25 µM AP-V, 20 µM gabazine).

*Organotypic brain slice culture.* Organotypic hippocampal slices cultures were prepared from postnatal day 6–8 Sprague-Dawley rats as described previously[64]. The brain was taken out and immediately placed in chilled dissection medium. Transverse hippocampal slices were cut with 400-µm thickness, and 4–6 slices were placed in a sterile culture plate insert (Millicell-CM, Millipore) in six-well plates containing prewarmed medium. Slices were biolistically transfected with a Helios Gene Gun (Bio-Rad) at DIV 2. Bullets were prepared using 12.5 µg of 1.6-µm gold particles and 80–100 µg of plasmid DNA. Slices were maintained until imaging at DIV 12–16.

Immediately before inverted imaging, slices were affixed to a nylon mesh weight and mounted upside down in a delta T brainslice adaptor for inverted microscope imaging (Bioptechs). Artificial cerebrospinal fluid (ACSF) was bubbled with carbogen (95% O$_2$, 5% CO$_2$) and flowed over the slice at 1 mL/min at 23 °C.

**Electrophysiology in neurons.** Measurements were performed on primary cultures at 13–15 DIV. Experiments were conducted in Tyrode's solution. Prior to imaging, neurons were incubated with 5 µM all-*trans* retinal for 30 min and then washed with Tyrode's solution.

Synaptic blockers were added to the imaging medium for measurements of single-cell electrophysiology. The blockers comprised NBQX (10 µM, Tocris), D(−)-2-amino-5-phosphonovaleric acid (AP-V; 25 µM, Tocris) and gabazine (SR-95531, 20 µM, Tocris). For measurements of channelrhodopsin photocurrents in neurons,

TTX (1 µM, Tocris) was included along with the synaptic blockers to prevent recruitment of voltage-gated sodium channels. Patch-clamp data were used if and only if access resistance was <25 MΩ and did not vary over the experiment. Recordings were terminated if membrane resistance changed by >10%. Experiments were performed at 23 °C under ambient atmosphere unless otherwise noted.

*Comparison of QuasArs to ArcLight A242.* ArcLight A242 was prepared in an identical lentiviral plasmid driven by a *CaMKIIα* promoter and was transfected (DIV 7) in parallel with the QuasAr plasmids in paired cultures. We used a standard ArcLight imaging intensity of 10 W/cm$^2$ at 488 nm. QuasAr expressing neurons were imaged at two intensities (300 and 800 W/cm$^2$). All recordings were made on the setup described below ("Optopatch measurements") at a 1 kHz frame rate. Due to its slow kinetics at room temperature (**Supplementary Fig. 6**), ArcLight recordings were made at 34 °C to enhance SNR and to match previously published conditions[16]. For comparisons in organotypic brain slice, ArcLight was imaged at 50 W/cm$^2$ on an upright microscope to enable simultaneous patch clamp stimulation and recordings. Recordings were made at a 1 kHz frame rate as described below ("Optopatch measurements") and were acquired at 34 °C.

**Immunostaining.** Cultures were fixed immediately following data acquisition in a solution of 4% paraformaldehyde and 4% sucrose (w/v) in PBS, pH 7.4 at room temperature for 8 min. Fixed cultures were then washed three times in Dulbecco's PBS supplemented with $Ca^{2+}$ and $Mg^{2+}$ (DPBS), pH 7.4, before permeabilization and blocking in a solution of 0.1% (w/v) gelatin and 0.3% Triton X-100 (v/v) in PBS, pH 7.4 (GTB), for 12–48 h at 4 °C.

For experiments using the sub-frame interpolation algorithm, primary cultures were fixed and stained using primary mouse monoclonal anti-ankyrinG (NeuroMab clone N106/36; 1:500), primary rabbit monoclonal anti-GFP (Abcam ab32146, lot YK011702CS, 1:1,000), secondary goat anti-rabbit Alexa Fluor 488–conjugated (Abcam ab150077, 1:500), and secondary goat anti-mouse Alexa Fluor 647–conjugated (Abcam ab150115, 1:500) antibodies.

For experiments on hiPSC-derived neurons, cultures were incubated with primary mouse anti-human nuclear antigen antibody (Millipore MAB1281 clone 235-1,1:500) in GTB overnight at 4 °C and then washed three times in DPBS and incubated with rabbit anti-GFP Alexa Fluor 488 conjugated (polyclonal, Life A21311, 1:300) and secondary antibody donkey anti-mouse Alexa Fluor 647 (Life A31571, 1:300) in GTB overnight at 4 °C. Cultures were washed three times in DPBS before mounting in DAPI Fluoromount-G (Southern Biotech).

**Optopatch measurements.** Experiments were conducted on a home-built inverted fluorescence microscope[17]. Briefly, illumination from a red laser (640 nm, 140 mW, Coherent Obis 637-140 LX) was expanded and focused onto the back focal plane of a 60× oil-immersion objective (NA 1.45, Olympus 1-U2B616). Imaging of brain slices was performed with a 20× water-immersion objective, NA 1.0 (Zeiss W Plan-Apo).

Illumination from a blue laser (488 nm, 50 mW, Omicron PhoxX) was sent through an acousto-optic modulator (AOM; Gooch and Housego 48058-2.5-.55-5W) for rapid control over the blue intensity. The beam was then expanded and modulated

by a digital micromirror device (DMD) with 608 × 684 pixels (Texas Instruments LightCrafter). The DMD was controlled via custom software (Matlab) through a TCP/IP protocol. The DMD chip was reimaged through the objective onto the sample, with the blue and red beams merging via a dichroic mirror. Each pixel of the DMD corresponded to 0.65 µm in the sample plane. A 532-nm laser was combined with the red and blue beams for imaging of mOrange2. We wrote software to map DMD coordinates to camera coordinates, enabling precise optical targeting of any point in the sample.

To achieve precise optical stimulation of user-defined regions of a neuron, it was necessary to determine the mapping from pixels on the DMD to pixels on the camera. A uniform fluorescent film (exc. 488 nm, em. 515 nm) was loaded into the microscope. The DMD projected an array of dots of known dimensions onto the sample. The camera acquired an image of the fluorescence. Custom software located the centers of the dots in the image and created an affine transformation to map DMD coordinates onto camera pixel coordinates.

A dual-band dichroic (Chroma zt532/635rpc) separated fluorescence of mOrange2 and Arch from excitation light. A 531/40-nm bandpass filter (Semrock FF01-531/40-25) and 495-nm longpass dichroic (Semrock FF495-Di03) was used for EGFP imaging, a 710/100-nm bandpass filter (Chroma, HHQ710/100) was used for Arch imaging, and a quad-band emission filter (Chroma ZET405/488/532/642m) was used for mOrange2 imaging and premeasurement calibrations. A variable-zoom camera lens (Sigma 18-200 mm f/3.5-6.3 II DC) was used to image the sample onto an EMCCD camera (Andor iXon+ DU-860), with 128 × 128 pixels. The variable zoom enabled imaging at a range of magnifications while maintaining the high light-collection efficiency of the oil- or water-immersion objectives.

In a typical experimental run, images of mOrange2 and QuasAr fluorescence were first acquired at full resolution (128 × 128 pixels). Data were then acquired with 2 × 2–pixel binning to achieve a frame rate of 1,000 frames/s. For experiments with infrequent stimulation (once every 5 s), the red illumination was on only from 1 s before stimulation to 50 ms after stimulation to minimize photobleaching. Cumulative red light exposure was typically limited to <5 min per neuron, although continuous red light exposure for 30 min was well tolerated (**Supplementary Fig. 5**). Full-resolution EGFP images were taken after functional recordings to prevent CheRiff excitation before the experiment.

Low-magnification wide-field imaging was performed with a custom microscope system based around a 2×, 0.5-NA objective (Olympus MVX-2). Illumination was provided by six lasers (640 nm, 500 mW, Dragon Lasers 635M500) combined in three groups of two. Illumination was coupled into the sample using a custom fused-silica prism, without passing through the objective. Fluorescence was collected by the objective, passed through an emission filter and imaged onto an sCMOS camera (Hamamatsu Orca Flash 4.0). This microscope imaged a 1.2 × 3.3–mm field of view with 3.25-µm spatial resolution and 2-ms temporal resolution, or a 4 × 4–mm field of view with 10-ms temporal resolution.

Blue illumination for channelrhodopsin stimulation was provided by a 473-nm, 1-W laser (Dragon Lasers) modulated in intensity by an AOM and spatially by a DMD (Digital Light Innovations DLi4130 – ALP HS). The DMD was reimaged onto the sample via the 2× objective. The DMD provided targeted

stimulation with excitation with 3.5-μm spatial resolution and 0.1-ms temporal resolution.

With either the high- or low-magnification microscope, a user then selected one or more regions of interest on the image and specified a time course for the illumination in each region. The software mapped the user-selected pixels onto DMD coordinates and delivered the illumination instructions to the DMD.

Illumination parameters for the data in **Figure 3** were as follows. **Figure 3b** blue illumination; 488 nm, 25 mW/cm$^2$, 10-ms pulses, repeated at 5 Hz. **Figure 3c** stimulation targeted to soma: 488 nm, 95 mW/cm$^2$, 10-ms pulses, repeated at 5 Hz. **Figure 3d** stimulation targeted to soma in ROI 1: 488 nm, 140 mW/cm$^2$, 10-ms pulses, repeated every 15 s. **Figure 3e** excitation targeted to dendrites: 488 nm, 100 mW/cm$^2$, 50-ms pulses, repeated at 5 Hz. The movie was constructed from an average of 203 temporally registered APs. **Figure 3e** whole-field stimulation: 488 nm, 0 to 10 mW/cm$^2$, 500-ms pulses, repeated at 6-s intervals. Synaptic blockers were added to suppress network activity.

**Data analysis.** *Statistics.* All error ranges represent s.e.m. unless otherwise specified. For two-sample comparisons of a single variable, data were tested for normality using the Shapiro-Wilk test. If the data were detectably non-Gaussian, we performed a nonparametric Mann-Whitney *U*-test. Otherwise we performed a two-tailed Student's *t*-test. Channelrhodopsin multiway comparisons of a single variable were made using a one-way ANOVA with Dunnett's *post hoc* test, using CheRiff as a reference. No channelrhodopsin data set was detectably non-Gaussian (Shapiro-Wilk). At probabilities $P < 0.05$, the null hypothesis was rejected and the results were judged statistically significant.

*Extracting fluorescence from movies.* Fluorescence values were extracted from raw movies in one of two ways. One approach used the maximum-likelihood pixel-weighting algorithm described previously[17]. Briefly, the fluorescence at each pixel was correlated with the whole-field average fluorescence. Pixels that showed stronger correlation to the mean were preferentially weighted. This algorithm automatically found the pixels carrying the most information, and de-emphasized background pixels. This approach was used for all experiments in cultured neurons and HEK293T cells. In images containing multiple neurons, the segmentation was performed semiautomatically using an independent components–based approach[65].

Alternatively, a user defined a region comprising the cell body and adjacent processes and calculated fluorescence from the unweighted mean of pixel values within this region. With the improved trafficking of the QuasAr mutants compared to that of Arch, the maximum-likelihood pixel-weighting algorithm was only marginally superior to manual definition of an ROI (**Supplementary Fig. 4**). For calculations of $\Delta F/F$ in HEK293T and neuron culture, background fluorescence from a cell-free region was subtracted from the baseline fluorescence of the cell. In measurements in brain slice, fluorescence was calculated from manually defined ROIs with equal pixel weighting and no background subtraction or correction for photobleaching.

*Precision of optically recorded AP timing.* To determine the temporal precision of the QuasAr indicators, we used a subframe interpolation algorithm[28,29] to infer the timing with which the fluorescence reached 70% of maximum at each AP, and compared this to simultaneously acquired high time-resolution patch-clamp recordings.

r.m.s. temporal jitter was 44 μs for QuasAr1 ($n = 97$ APs) and 61 μs for QuasAr2 ($n = 99$ APs). This jitter reflects the combined errors in timing intrinsic to the optical measurement (shot noise and distortion of the waveform by the reporter) and errors introduced by temporal discretization of the camera frames and the subframe interpolation. Thus optical recordings with QuasArs can determine spike timing with precision much greater than the camera exposure time.

*Fitting channelrhodopsin photocurrents.* Photocurrents of the channelrhodopsins were characterized following previously described protocols[24]. Briefly, peak photocurrents in response to a light pulse (488 nm, 0.5 W/cm$^2$, 1-s duration) were identified by first smoothing the traces using robust Loess method with a filter width of 2 ms and then finding the extremum of the filtered trace after laser onset and subtracting the baseline current. Time to peak ($t_{on}$) was defined as the time between light onset and peak photocurrent of the filtered trace. The steady-state photocurrent was found by fitting a monoexponential curve to the filtered trace from 2 ms after the peak until laser offset. The offset of this fit was defined as the steady-state photocurrent. The time constant of this fit was defined as the desensitization rate ($\tau_{des}$). The channel closure rate ($\tau_{off}$) in response to a light pulse (488 nm, 0.5 W/cm$^2$, 5-ms duration) was measured by fitting a monoexponential to the decay of the photocurrent after light offset.

Illumination intensities for 50% effective light power density[24] (EPD50; **Supplementary Table 4**) values were determined from measurements of peak photocurrents versus a series of whole-field illumination intensities. For each cell, peak photocurrents at each intensity were first normalized by the maximum peak photocurrent. The resulting curves were then fitted with a simple binding model ($Y = B_{max} \times X / (EPD50 + X)$). The reported EPD50s are the average of the fit parameters from $n = 5$ cells.

**Subframe interpolation of AP timing.** The subframe interpolation algorithm consists of a series of computational image-processing steps (**Supplementary Fig. 13**). Each step may be modified to account for experiment-specific attributes of the data.

A neuron was induced to fire through repeated optical stimulation of a user-selected subcellular compartment (typically soma or dendrite). We typically observed 5% photobleaching over a 40-s acquisition. Photobleaching was typically dominated by nonspecific background fluorescence rather than by photobleaching of QuasAr, and often photobleaching did not follow a simple single-exponential decay. The photobleaching baseline was constructed from the whole-field intensity by a sliding minimum filter, followed by a sliding mean filter. Each frame of the movie was then corrected by dividing by this baseline.

QuasAr fluorescence intensity $F(t)$ was determined either by the regression algorithm described before[17] or by whole-field average intensity. Both procedures gave similar results, with slightly better SNR returned by the regression algorithm (**Supplementary Fig. 4**).

Determination of spike times was performed iteratively. A simple threshold-and-maximum procedure was applied to $F(t)$ to determine approximate spike times, $\{T_0\}$. Waveforms in a brief window bracketing each spike were averaged together to produce a preliminary spike kernel $K_0(t)$. We then calculated the cross-correlation of $K_0(t)$ with the original intensity trace $F(t)$. Whereas the timing of maxima in $F(t)$ was subject to errors from single-frame noise, the peaks in the cross-correlation, located

at times {$T$}, were a robust measure of spike timing. A movie showing the mean AP propagation was constructed by averaging movies in brief windows bracketing spike times {$T$}. Typically, 100–400 APs were included in this average. The AP movie had high SNR but did not clearly show signal propagation.

We applied spatial and temporal linear filters to further decrease the noise in the AP movie. The spatial filter consisted of convolution with a Gaussian kernel, typically with an s.d. of 1 pixel. The temporal filter was based upon principal-components analysis (PCA) of the set of single-pixel time traces. The time trace at each pixel was expressed in the basis of PCA eigenvectors. Typically, the first five eigenvectors were sufficient to account for >99% of the pixel-to-pixel variability in AP waveforms, and thus the PCA eigendecomposition was truncated after five terms. The remaining eigenvectors represented uncorrelated shot noise (**Supplementary Fig. 13b**). Projections of the movie onto the PCA eigenvectors showed only spatial features above noise for the first five eigenvectors (**Supplementary Fig. 13c** inset). To verify that the spatial and PCA filtering did not distort the underlying AP waveforms, we compared mean AP waveforms in subcellular compartments before and after the smoothing steps (**Supplementary Fig. 13d**). We observed no systematic deviations in the AP waveforms in the axon, soma or dendrites.

The user then set a threshold depolarization to track (represented as a fraction of the maximum fluorescence transient), and a sign for d$V$/d$t$ (indicating rising or falling edge). We chose 50% maximal depolarization on the rising edge. The filtered data were fit with a quadratic spline interpolation, and the time of threshold crossing was calculated for each pixel to create a map of the AP delay (**Supplementary Fig. 13e**).

The subframe timing precision of the algorithm was calibrated by patch-clamp measurements. Optically induced APs were recorded simultaneously via QuasAr1 fluorescence in the soma and by conventional patch clamp, also in the soma (**Supplementary Fig. 13f**). The r.m.s. error in timing was 54 μs in this instance and did not show systematic bias at the frame boundaries.

The fits were converted into movies showing AP propagation as follows. Each pixel was kept dark except for a brief flash timed to coincide with the timing of the user-selected AP feature at that pixel. The flash followed a Gaussian time course, with amplitude equal to the local AP amplitude and with duration equal to the cell-average time resolution, σ. Frame times in the subframe interpolation movies were selected to be approximately twofold shorter than σ.

Occasionally it was possible to enhance the spatial resolution of the high–temporal resolution movies by mapping the timing data onto a higher–spatial resolution static image of fluorescence of EGFP (from the CheRiff-EGFP fusion, **Supplementary Fig. 13g**) or of QuasAr1. The pixel matrix of the subframe interpolated movie was expanded to match the dimensions of the high-resolution image, and the amplitude at each pixel was then set equal to the mean brightness at that pixel. Selected frames from the resulting movie showed AP initiation at the axon initial segment in the first two frames (**Supplementary Fig. 13h** and **Supplementary Video 4**). For assembly of the color movies (**Fig. 3e**, **Supplementary Fig. 13** and **Supplementary Videos 4–6**), the timing signal was assigned to a color map that was overlaid on a grayscale image of mean QuasAr fluorescence. Optionally, the optically stimulated region of the cell was highlighted in blue.

47. Zhao, H., Giver, L., Shao, Z., Affholter, J.A. & Arnold, F.H. Molecular evolution by staggered extension process (StEP) *in vitro* recombination. *Nat. Biotechnol.* **16**, 258–261 (1998).
48. Zhao, Y. *et al.* An expanded palette of genetically encoded Ca$^{2+}$ indicators. *Science* **333**, 1888–1891 (2011).
49. Cheng, Z. & Campbell, R.E. Assessing the structural stability of designed β-hairpin peptides in the cytoplasm of live cells. *ChemBioChem* **7**, 1147–1150 (2006).
50. Lanyi, J.K. Proton translocation mechanism and energetics in the light-driven pump bacteriorhodopsin. *Biochim. Biophys. Acta* **1183**, 241–261 (1993).
51. Lanyi, J.K. Bacteriorhodopsin. *Annu. Rev. Physiol.* **66**, 665–688 (2004).
52. Kolodner, P., Lukashev, E.P., Ching, Y. & Rousseau, D.L. Electric-field-induced Schiff-base deprotonation in D85N mutant bacteriorhodopsin. *Proc. Natl. Acad. Sci. USA* **93**, 11618–11621 (1996).
53. Ma, D. *et al.* Role of ER export signals in controlling surface potassium channel numbers. *Science* **291**, 316–319 (2001).
54. Gradinaru, V. *et al.* Molecular and cellular approaches for diversifying and extending optogenetics. *Cell* **141**, 154–165 (2010).
55. Kirkton, R.D. & Bursac, N. Engineering biosynthetic excitable tissues from unexcitable cells for electrophysiological and cell therapy studies. *Nat. Commun.* **2**, 300 (2011).
56. Park, J. *et al.* Screening fluorescent voltage indicators with spontaneously spiking HEK cells. *PLoS ONE* **8**, e85221 (2013).
57. Pucihar, G., Kotnik, T. & Miklavčič, D. Measuring the induced membrane voltage with di-8-ANEPPS. *J. Vis. Exp.* **33**, e1659 (2009).
58. Enami, N. *et al.* Crystal structures of archaerhodopsin-1 and-2: common structural motif in archaeal light-driven proton pumps. *J. Mol. Biol.* **358**, 675–685 (2006).
59. Barondeau, D.P., Putnam, C.D., Kassmann, C.J., Tainer, J.A. & Getzoff, E.D. Mechanism and energetics of green fluorescent protein chromophore synthesis revealed by trapped intermediate structures. *Proc. Natl. Acad. Sci. USA* **100**, 12111–12116 (2003).
60. McCarthy, K.D. & de Vellis, J. Preparation of separate astroglial and oligodendroglial cell cultures from rat cerebral tissue. *J. Cell Biol.* **85**, 890–902 (1980).
61. Banker, G. & Goslin, K. *Culturing Nerve Cells* (MIT Press, 1998).
62. Chen, G., Harata, N.C. & Tsien, R.W. Paired-pulse depression of unitary quantal amplitude at single hippocampal synapses. *Proc. Natl. Acad. Sci. USA* **101**, 1063–1068 (2004).
63. Jiang, M. & Chen, G. High Ca$^{2+}$ -phosphate transfection efficiency in low-density neuronal cultures. *Nat. Protoc.* **1**, 695–700 (2006).
64. Stoppini, L., Buchs, P.-A. & Muller, D. A simple method for organotypic cultures of nervous tissue. *J. Neurosci. Methods* **37**, 173–182 (1991).
65. Mukamel, E.A., Nimmerjahn, A. & Schnitzer, M.J. Automated analysis of cellular signals from large-scale calcium imaging data. *Neuron* **63**, 747–760 (2009).